

UNCLASSIFIED

AD NUMBER

AD908713

LIMITATION CHANGES

TO:

Approved for public release; distribution is unlimited. Document partially illegible.

FROM:

Distribution authorized to U.S. Gov't. agencies only; Test and Evaluation; 03 APR 1973. Other requests shall be referred to Army Mobility Equipment Research and Development Center, Attn: STSFB, Fort Belvoir, VA 22060. Document partially illegible.

AUTHORITY

USAMERDC Itr, 11 Oct 1973

THIS PAGE IS UNCLASSIFIED

**Best
Available
Copy**

AD 008713 L

TRW
SYSTEMS GROUP

AD 908713

TRW Report AT-73-2
23 February 1973

LAND MINE DETECTION SYSTEM
FINAL REPORT

Prepared by
Allen M. Morita
Advanced Technology Staff
Space Vehicles Division

Prepared for
U.S. Army Mobility Equipment Research and Development Center
Ft. Belvoir, Virginia 22060
Under Contract No. DAAK02-72-C-0340

attr STSFB

Sponsored by Defense Advanced Research Projects Agency
(ARPA Order No. 2011)

*Distribution limited to U.S. Gov't. agencies only!
Test and Evaluation; 3 APR 1973
For this document must be referred to
Center 3010 Other reports*

DDC
RECORDED
APR 2 1973
REGULATED
B

TRW SYSTEMS GROUP
One Space Park
Redondo Beach, California 90278

The findings in this report are not to be construed as an official Department of the Army position unless so designated by other authorized documents.



TRW Report AT-73-2
23 February 1973

LAND MINE DETECTION SYSTEM

FINAL REPORT

Prepared by

Allen M. Morita
Advanced Technology Staff
Space Vehicles Division

Prepared for

U.S. Army Mobility Equipment Research and Development Center
Ft. Belvoir, Virginia 22060
Under Contract No. DAAK02-72-C-0340

Sponsored by Defense Advanced Research Projects Agency
(ARPA Order No. 2011)

TRW SYSTEMS GROUP
One Space Park
Redondo Beach, California 90278

The findings in this report are not to be construed as an official Department of the Army position unless so designated by other authorized documents.

FOREWORD

The work reported here was performed by the Advanced Technology Staff of the Space Vehicles Division. It was sponsored by the Defense Advanced Research Projects Agency under ARPA Order No. 2011. Technical monitor for the contract was Dr. Huey Roberts of the Mine Detection Division, U.S. Army Mobility Equipment Research and Development Center. Technical comments and suggestions made by Dr. Huey Roberts and Dr. Karl Steinbach, U.S. Army Mobility Equipment Research and Development Center; Dr. Charles H. Church of Defense Advanced Research Projects Agency; and Dr. R. L. Johnson and Dr. P. G. Bhuta of TRW Systems Group; are acknowledged. Valuable assistance provided by J. E. Martija in performance of the tests throughout the course of the contract is also acknowledged.

ABSTRACT

Since land mines appear in both metallic and nonmetallic forms, a mine detection system is needed which does not depend significantly on the materials from which the mines are constructed. Reflection of acoustic waves from buried objects could provide a physical basis for such a detection system. The objective of this contract was to determine the feasibility of using acoustic waves for land mine detection.

The contract approach to determining the feasibility of acoustic land mine detection was developed in two phases. The first phase was to conduct acoustic tube tests on soils to determine sound velocity and attenuation as a function of frequency and soil moisture content. The next phase consisted of static in-situ reflection tests to determine the ability of acoustic waves to detect buried metallic, nonmetallic simulated mines and rocks. Surface wave interference was also investigated.

A probing frequency of 3 KHz yielded the best reflection signals at probing depths exceeding 12 inches. The reflected signals from all of the simulated mines were significantly above background noise. The mine reflected signals exhibited a signature significantly different from those obtained with no mine present and with small soil inhomogeneities present. Rock reflected signals generally exhibited irregular axes of reflection.

As a result of mine reflection tests, it is evident that acoustic waves can be used for a land mine detection system. Mine reflected acoustic signals can be detected and imaged from both nonmetallic and metallic mines at the burial depths most likely occurring in a field situation.

One of the appealing features of the acousto-optical imaging mine detection system is that it can also be used in shallow water near shorelines where other types of mine detection systems, such as microwaves, do not function in the presence of water. Hence the incorporation of an acoustic imaging subsystem, in a total mine detection system consisting of more than one subsystem, would provide a more complete mine detection capability under different environmental and soil conditions that are likely to be encountered. The imaging feature should discriminate between mines and other naturally occurring inhomogeneities in soils and hence significantly reduce the number of false alarms per area swept.

TABLE OF CONTENTS

	<u>Page</u>
1.0 INTRODUCTION.	1
1.1 Summary of Results	2
1.2 Conclusions.	3
1.3 Recommendations.	4
2.0 TUBE TESTS.	6
2.1 Tube Tests on Sand	13
2.2 Tube Tests on Sand-Clay Mixture.	18
3.0 REFLECTION TESTS.	25
3.1 Mine Reflection Tests.	41
3.2 Acoustic Impedance	66
4.0 REFERENCES.	71

LIST OF ILLUSTRATIONS

<u>Figure</u>		<u>Page</u>
1	Particle size distribution, sand.	7
2	Particle size distribution, sand-clay mixture	8
3	Tube test, sensor configuration	9
4	Tube test, instrumentation configuration.	10
5	Pulse signal input to transducer.	11
6	Tube test, accelerometer response, 3 and 10 KHz	12
7	Attenuation in sand	19
8	Attenuation in sand	20
9	Test site	26
10	Test pit, empty	26
11	Test pit, filled.	27
12	Moisture cell placement in pit.	27
13	Particle size distribution for sand in large test pit	28
14	Instrumentation configuration	29
15	Frequency spectrum, 1.6 KHz signal input.	30
16	Frequency spectrum, received 1.6 KHz signal	31
17	Frequency spectrum, received 1.6 KHz signal	32
18	Frequency spectrum, 3 KHz signal input.	33
19	Frequency spectrum, received 3 KHz signal	34
20	Frequency spectrum, received 3 KHz signal	35
21	Frequency spectrum, 10 KHz signal input	36
22	Frequency spectrum, received 10 KHz signal.	37
23	Frequency spectrum, received 10 KHz signal.	38
24	Accelerometer response, 1.6 KHz	40
25	Accelerometer response, 3.0 KHz	40
26	Accelerometer response, 10 KHz.	41
27	Transmitting and receiving transducers.	42
28	Reflection test instrumentation configuration	42
29	Reflection test layouts	44
30	Simulated wooden mine	45
31	Simulated steel mine, 1/16" plates.	45
32	Simulated steel mine, 1/4" plates	46

LIST OF ILLUSTRATIONS (Cont.)

<u>Figure</u>	<u>Page</u>
33 Plastic block	46
34 Simulated wax mine.	47
35 Simulated soil inhomogeneity.	47
36 Large rock used for reflection tests.	48
37 Small rock used for reflection tests.	48
38 Reflected signal, steel plate, 9" depth, 10 KHz	49
39 Reflected signal, steel plate, 9" depth, 3 KHz.	49
40 Reflected signal, steel plate, 9" depth, 1.6 KHZ.	50
41 Reflected signal, wooden mine, 9" depth, 10 KHz	51
42 Reflected signal, wooden mine, 9" depth, 3 KHz.	51
43 Reflected signal, wooden mine, 9" depth, 1.6 KHz.	52
44 Reflected signal, plastic block, 9" depth, 3 KHz.	52
45 Reflection test configuration utilizing accelerometers.	54
46 Traces from buried accelerometers	54
47 Reflected signal, wooden mine, 12" depth, 3 KHz	55
48 Traces from buried accelerometers	56
49 Reflected signal, wooden mine, 12" depth, 3 KHz	56
50 Reflected signal, plastic block, 12" depth.	57
51 Reflected signal, steel, 1/4" plates, 12" depth	57
52 Reflected signal, steel, 1/16" plates, 12" depth.	58
53 Reflected signal, wax block, 11" depth.	58
54 Reflected signal, large rock, 9" depth.	59
55 Reflected signal, small rock, 6" depth.	59
56 Reflected signal, pocket of clay, 6" depth.	61
57 Signal received with nothing buried	61
58 Reflected signal, steel, 1/4" plates, 9" depth.	64
59 Reflected signal, steel, 1/16" plates, 9" depth	64
60 Transmission through a separating material.	66
61 Thin piece of material with soil on one side and air on the opposite site	70

LIST OF TABLES

<u>Table</u>		<u>Page</u>
I	Tube test, sand moisture content	13
II	Sound velocities in sand	14
III	Wavelengths of sound in sand	15
IV	Attenuation in sand.	17
V	Moisture content, sand-clay mixture.	21
VI	Sound velocities, sand-clay mixture.	22
VII	Attenuation, sand-clay mixture	23
VIII	Reflection test measurements	62
IX	Characteristic impedance	67
X	Transmission from water through rubber into soil	68
XI	Sound power reflection coefficient for mines buried in soil. .	69
XII	Sound power reflection coefficient for thin mine material backed by air cavity	70

1.0 INTRODUCTION

Since land mines appear in both metallic and nonmetallic forms, a mine detection system is needed which does not depend significantly on the materials from which the mines are constructed. Reflection of acoustic waves from buried objects could provide a physical basis for such a detection system. The objective of this contract was to determine the feasibility of using acoustic waves for the design of an acoustic imaging system suitable for land mine detection.

The utilization of acoustic waves can provide a real-time mine imaging system applicable to several soils and soil conditions. The acoustic detection method has the advantage of increasing detection capability as the soil moisture content increases, whereas the detection capability of other methods decreases with increasing moisture content. In any mine detection system it is necessary to distinguish between the signal from a mine and other naturally occurring objects, otherwise a high false alarm rate results. The acoustic imaging system has the potential to discriminate between a mine and a naturally occurring object by its capability of providing images of objects underground. This imaging ability reduces the amount of operator training necessary to interpret the image display.

The contract approach to determining the feasibility of acoustic land mine detection was developed in two phases. The first phase was to conduct acoustic tube tests on sand and a sand-clay mixture. These tests led to a determination of acoustic wave velocity and attenuation as a function of probing frequency and soil moisture content. The next phase consisted of static in-situ reflection tests to determine the ability of acoustic waves to detect buried metallic and nonmetallic simulated mines. The material composition of the mines simulated were wood, steel, plastic and wax. Reflection tests were also made on rocks and a pocket of clay in sand. The objectives of these tests were to determine (1) the mine material dependence of the reflected wave, (2) if acoustic waves yielded adequate mine probing depths, (3) the extent of reflected signals from naturally occurring objects, and (4) the extent of reflected signals from small soil

inhomogeneities. Since source generated waves traveling along the surface were thought to be a potential problem in discrimination of a mine reflected signal, surface wave interference was investigated.

1.1 Summary of Results

The tube tests on sand and the sand-clay mixture yield sufficient data on sound velocity and attenuation to qualitatively predict the capability of obtaining a usable reflected signal from mines buried in soils of these types. These preliminary tests on a soil sample aid in determining a suitable probing frequency for the reflection tests. The results obtained during these tests adequately portrayed the acoustic wave behavior obtained at the in-situ test site.

The sound velocity in sand was 583 ft/sec and did not vary with frequency or soil moisture content. As expected, the acoustic attenuation increased with increasing probing frequency. Increasing soil moisture content near the surface provides for better coupling of the acoustic signal into the soil but the increase in mass due to increasing water content appeared to attenuate the acoustic wave to a greater extent below the surface. The net effect of increasing moisture content, however, was to increase the signal amplitudes in the soil.

The sound velocity in the sand-clay mixture was 470 ft/sec in the dry soil and increased to approximately 840 ft/sec in soil at a moisture content of 8%. The attenuation was more severe in the mixture than for the pure sand.

The reflected signals from all of the simulated mines were significantly above background noise at mine burial depths up to 12 inches. Deeper probing depths appeared to be possible but were not attempted since typical field burial depths of anti-tank mines range from 5 to 8 inches. As the soil moisture content was increased, so did the amplitudes of the reflected signals. It was evident that the prime moisture effect was dependent on the moisture content of the surface soil. If the surface and the soil below were moist, the reflection signals were large. If the surface was dry but the soil below was moist, then the reflection signals were somewhat smaller. Thus, as the surface moisture content increases, more of the acoustic radiated power is propagated into the soil.

A probing frequency of 3 KHz yielded the best reflection signals with adequate probing depths. A lower frequency of 1.6 KHz resulted in a longer wavelength. This longer wavelength resulted in the mine barely appearing as a discontinuity in the soil, thus the reflection signals were of poorer quality than those of the 3 KHz frequency. The 10 KHz frequency was too highly attenuated to yield an adequate probing depth.

The reflected signals from the rocks depend significantly on their orientation relative to the surface. Since the rocks were generally irregular in shape, they tend to scatter more of the incident acoustic wave. The amount of signal reflected back to the surface was generally dependent on the largest cross-sectional area parallel to the surface. If this cross-section was triangular in shape, the largest reflection signal was obtained approximately along the axis of the longest side. When an attempt was made to reflect an acoustic wave from a small pocket of clay in sand, no reflected signals were received. The received signal was almost identical to that obtained when no object was buried in a homogeneous sand.

Investigations into the extent of interference caused by surface waves revealed that (1) when the surface was dry and loose, a very small amplitude wave was propagated along the surface from transmitter to receiver, (2) when the surface moisture content was increased, a larger amplitude surface wave was apparent, (3) increasing the surface moisture content resulted in better acoustic coupling yielding larger reflection signals, and (4) if the surface wave amplitude increased, the reflected signal amplitude also increased. The net observation was that the reflected signal could be easily discerned from the surface wave because of its larger relative amplitude. No interference of any significance was obtained due to the surface wave.

1.2 Conclusions

Acoustic waves can be used for a land mine detection system. Mine reflected acoustic signals can be received from both nonmetallic and metallic mines at the burial depths most likely occurring in a field situation. The mine material factor appears to be less of a constraint in obtaining mine reflected signals than are the soil composition and moisture content. A rough observation would be that the soil particle size and soil density

determine to a large extent what the most promising probing frequency would be. The soil moisture content is related to how much of the signal enters the soil and how large a mine reflected signal is incident on the receiver.

Due to the rather irregular scattering of the probing acoustic signal by rocks, it appears that irregularly shaped rocks will appear irregular when imaged. Since small soil inhomogeneities do not differ significantly in acoustic impedance (as compared to the soil-mine impedance mismatch) from that of the host soil, reflected signals from these inhomogeneities are at best very slight. Surface wave interference did not pose any problems in discerning the mine reflected signal. It appears that minimal circuit design, if any, is all that would be required to eliminate this type of noise from the processed signal.

The objectives of the contract have been met. Acoustic waves are a technically feasible method of detecting buried anti-vehicular mines. In-situ test results indicate that mine reflected acoustic waves can be processed to yield a real-time image of buried mines. Discrimination of these imaged mines from naturally occurring rocks appears possible. Since imaging was not a part of this contract, however, this assertion must be proven by actual field testing.

1.3 Recommendations

The in-situ mine reflection test data and analysis indicate that acoustic waves may be used in a land mine detection system. Preliminary studies into a field deployable system indicate that a feasible system can be developed to meet field requirements. The system could be used to detect anti-vehicular mines and large anti-personnel mines whose detonation pressures are within the design limitations of the system.

The results and conclusions of this contract are based on static in-situ tests. Since the field deployed system must move along the ground, detection capability should be verified under these conditions. Tests conducted in this manner would also aid in characterizing other system implementation areas.

One of the appealing features of the acousto-optical imaging mine detection system is that it can also be used in shallow water near shorelines where other types of mine detection systems, such as microwaves, do not function in the presence of water. Hence the incorporation of an acoustic imaging subsystem, in a total mine detection system consisting of more than one subsystem, would provide a more complete mine detection capability under different environmental and soil conditions that are likely to be encountered. The imaging feature should discriminate between mines and other naturally occurring inhomogeneities in soils and hence significantly reduce the number of false alarms per area swept.

2.0 TUBE TESTS

The objectives of the tube tests were to determine the velocity and attenuation of acoustic waves propagated in a sample of soil. The analysis of wave propagation in a sample can be performed under controlled laboratory conditions and yields sufficient information to be of use in predicting wave behavior under in-situ conditions. The tube tests can indicate a frequency range to examine for use in mine detection and also develop some qualitative information as to wave behavior as the moisture content increases.

The tube tests were conducted on sand and a sand-clay mixture. The mixture was prepared in the ratio of six parts sand to one part clay by weight. Sieve analyses were conducted on random samples of the soils. Figures 1 and 2 illustrate the particle size distributions by weight of the sand and sand-clay mixture, respectively. Seven sieve screens were used; U.S. Standard Sieve Series numbers 10, 18, 35, 40, 60, 140 and 200. Since the clay is very cohesive and thus sticks to the larger sand particles, the particle distribution of Figure 2 should exhibit a higher percentage in the 140-200 micron screens than the sieve analysis revealed. The initial dry density of the sand was 114 pounds per cubic foot. The initial dry density of the sand-clay mixture was 109 pounds per cubic foot.

Accelerometers were buried in the soil to measure the wave propagation into the soil. Moisture cells were also buried. Figure 3 indicates the placement of accelerometers and moisture cells within the tube. A1, A2, A3, and A4 are the accelerometers and M1, M2, and M3 are the soil temperature-moisture cells. Figure 4 illustrates the test instrumentation configuration.

The sound velocity measurements were made using a conventional pulse technique. A repetitive signal of a two (or more) cycle burst, at the transducer's resonant frequency, followed by no signal for 128 cycles was applied to the transducer. As an example, a pulse signal applied to the 3.0 KHz transducer is illustrated in Figure 5. The long "off" time of 128 cycles was used so that all reflection arrivals could be discerned before application of the next burst of 2 cycles. Referring to the accelerometer designations in Figure 3, the arrival time of the first positive

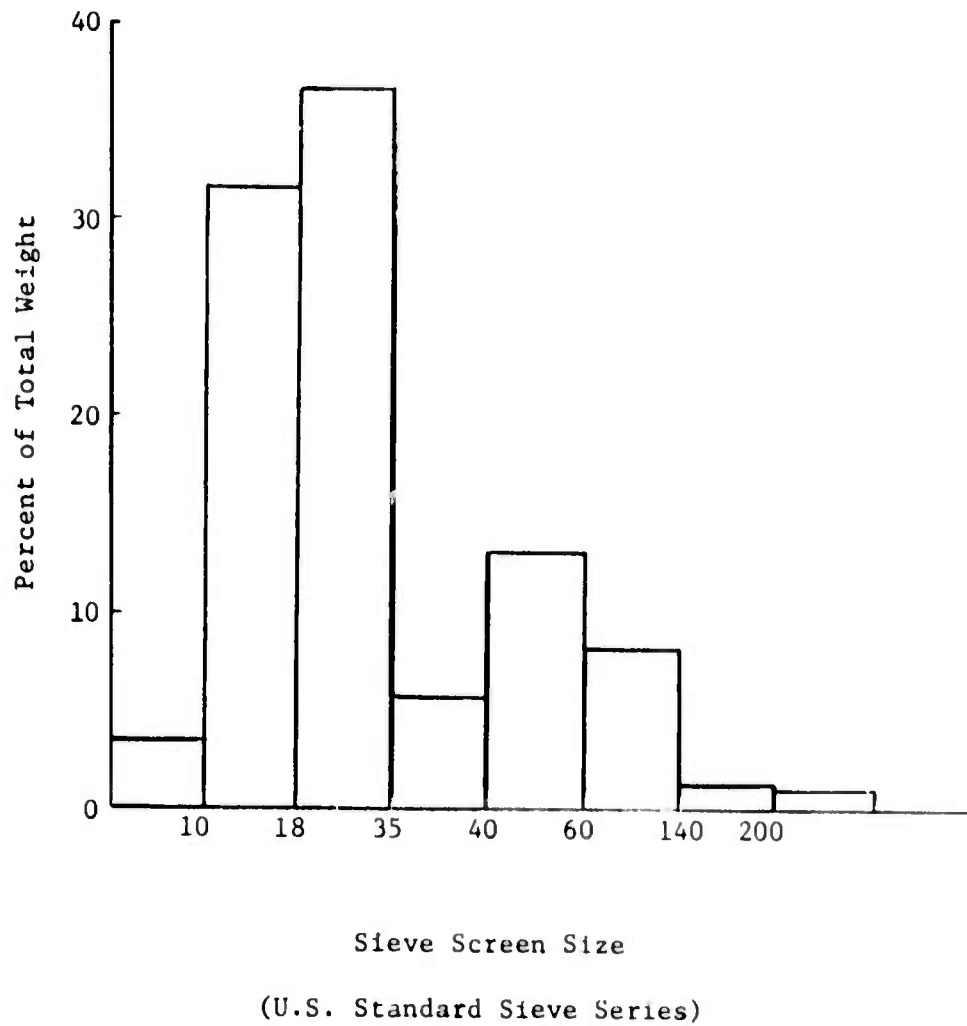


Figure 1: Particle size distribution for builder's sand.

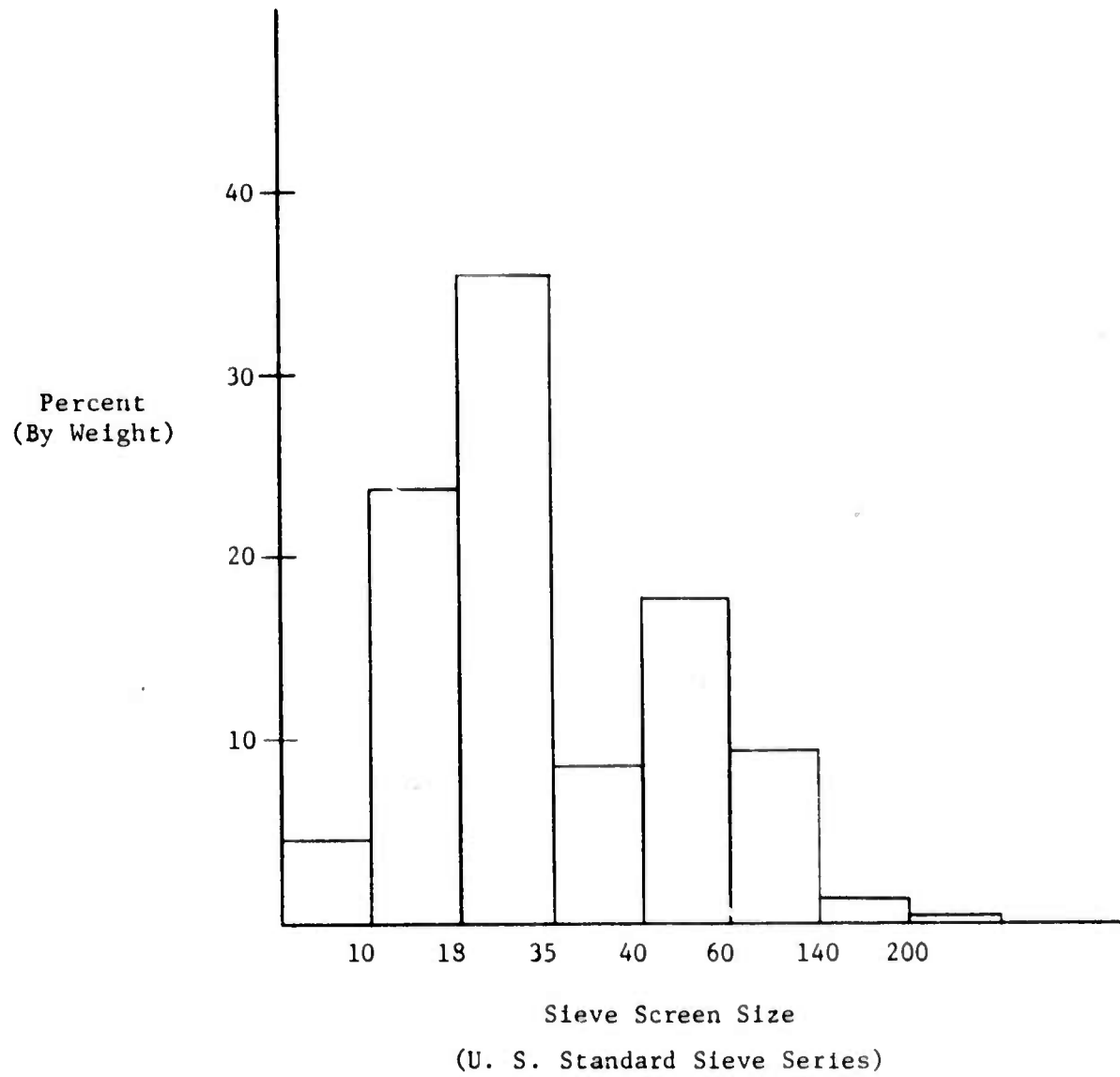


Figure 2: Particle size distribution for sand-clay mixture.

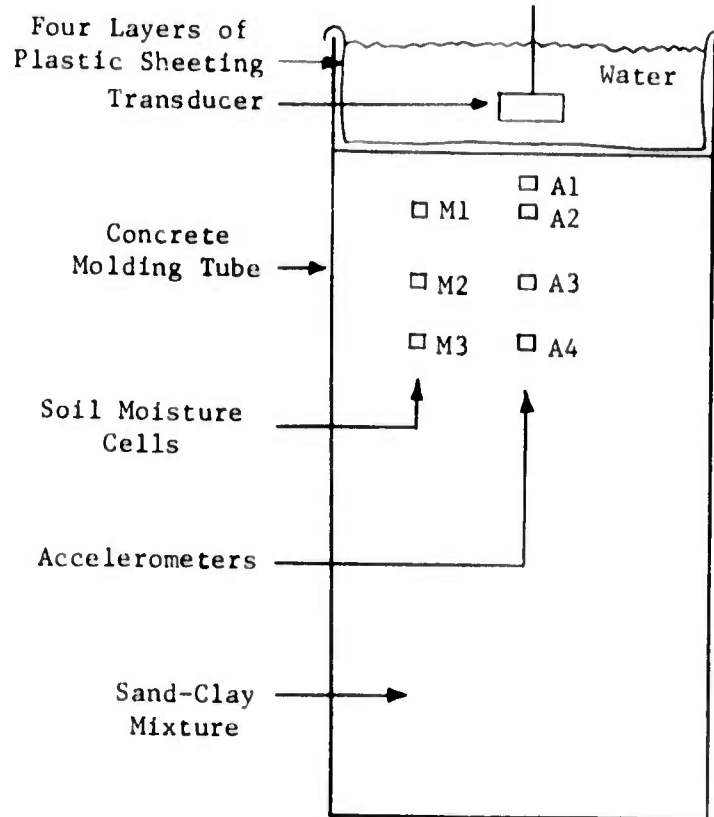


Figure 3: Tube test accelerometer and soil moisture cell placement.

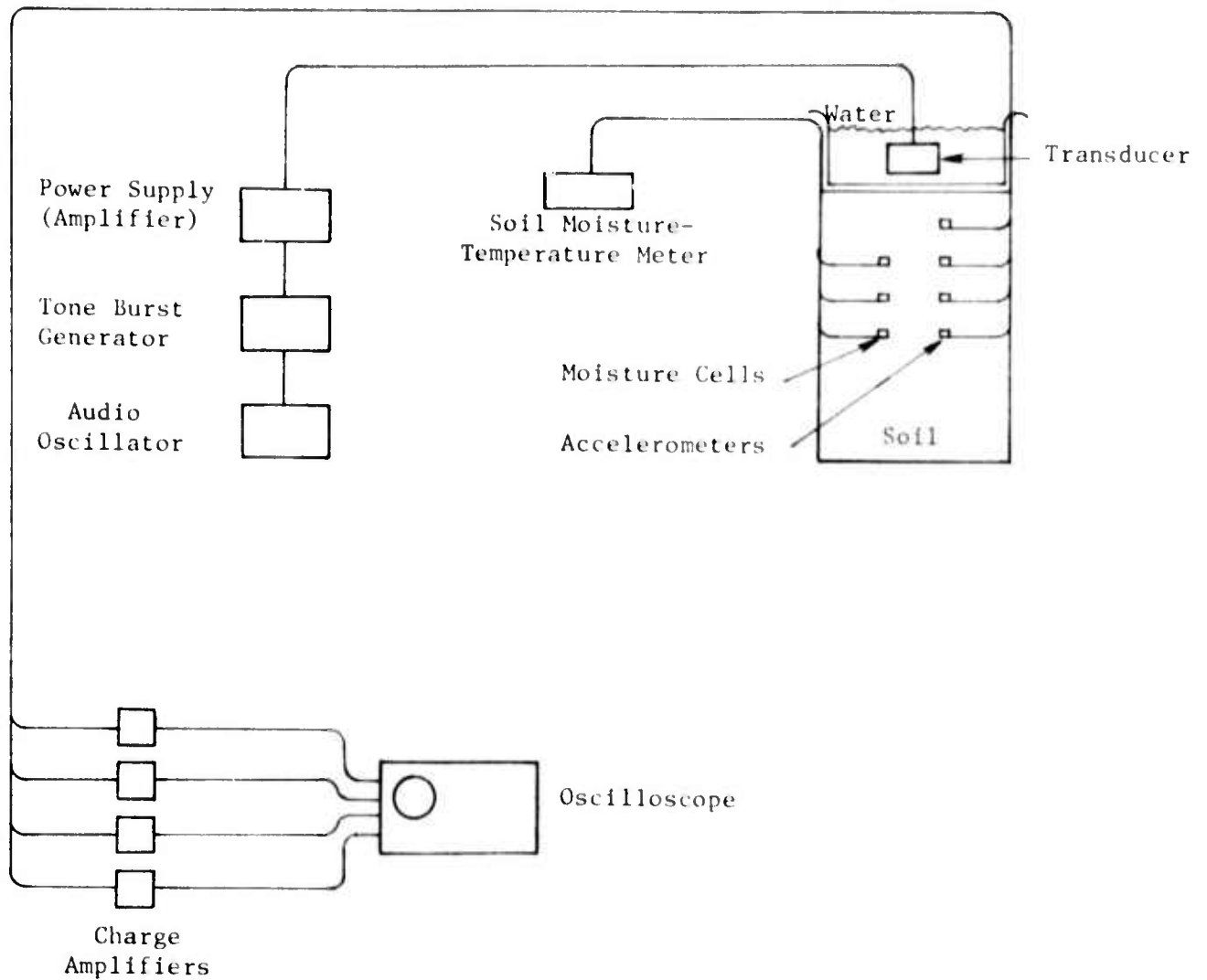


Figure 4: Tube test instrumentation configuration.

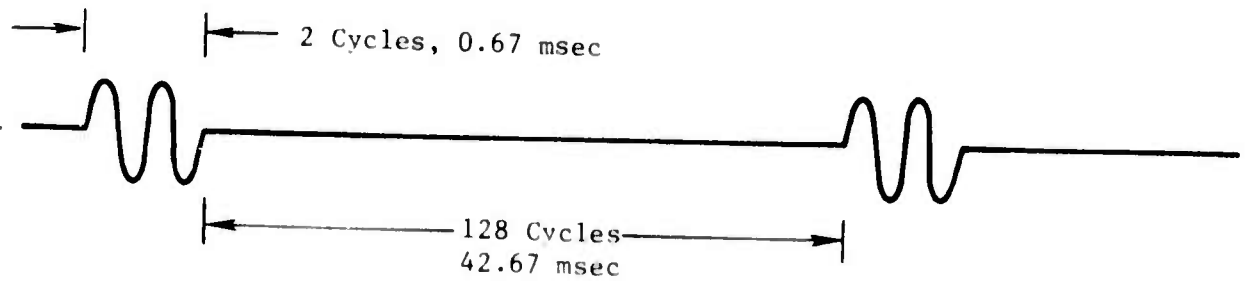


Figure 5: Pulse signal input to 3.0 KHz transducer.

half cycle of accelerometers #A2, A3 and A4 were referenced to the first positive half cycle received at accelerometer #A1. Figure 6a is an example of the output waveforms of the accelerometers, in this case the response to a burst of 2 cycles at 3 KHz. Figure 6b is an example of the waveform obtained when a 10 KHz pulsed signal was utilized. Notice that the high frequency signal is totally lost by the time it reaches the bottom accelerometer, only the low frequency component is received.

When the time displacement measurements were made, the oscilloscope's horizontal time base was expanded as much as possible to make more accurate measurements. The velocity was calculated by dividing the distance between two accelerometers by the difference in the time of arrival of the first positive half cycle.

The attenuation measurements were made by applying a continuous wave signal (at the transducer's resonant frequency) to the sound projecting transducer. The amplitudes of the accelerometer's output responses were then measured. The attenuation was then converted to a loss in decibels/inch by the equation:

$$\text{Attenuation} = 20 \log_{10} \frac{A_i}{A_1} \div \text{distance between accelerometers}$$

where A_1 = the amplitude of the output signal from accelerometer #A1

A_i = the amplitude of the output signal from accelerometers #A2, A3 and A4.

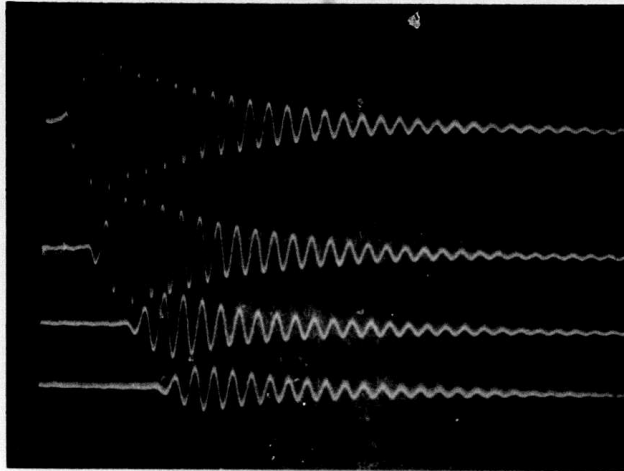


Figure 6a: Response of accelerometers to a burst of 2 cycles at 3 KHz. From top to bottom, the traces are the outputs of accelerometers #A1 thru #A4. The vertical scale is 0.05 volt/division for each trace. Horizontal scale: 1 msec/division.

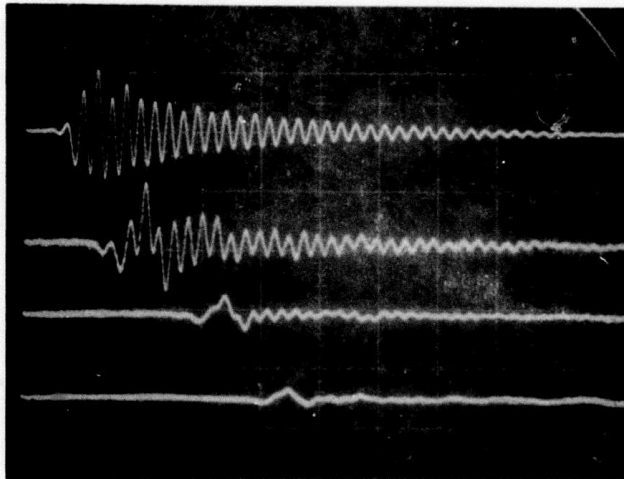


Figure 6b: Response to a burst of 2 cycles at 10 KHz. Horizontal scale - 0.5 msec/division, vertical scale - 0.5 volt/division (top trace), 0.05 volt/division (bottom three traces). From top to bottom traces are the responses from accelerometers #A1 to #A4.

When a standing wave situation was evident the pulse amplitudes were used in calculation of the attenuation. This situation occurred primarily when the 1.6 KHz frequency was used. The moisture content was varied by even watering of the top surface.

2.1 Tube Tests on Sand

The moisture content of the sand during the tube tests is given in Table I. Table II is a complete list of the sound velocities calculated.

TABLE I. Moisture Content, Builder's Sand

TEST NUMBER	MOISTURE CONTENT, % WATER BY WEIGHT			
	#M1	#M2	#M3	#M4
1	0	0	0	0
2	4	3	0	0
3	4	4	0	0
4	4	3	3	3
5	4	3	3	3
6	4	3	3	3
7	3	3	3	4
8	4	4	3	3
9	4	4	4	4
10	4	4	4	4
11	4	4	4	4
12	3	3	4	4

The velocity tolerance is $\pm 18\%$ for those velocities calculated between #A1 and #A2; $\pm 7\%$ for those velocities calculated between accelerometers #A1 and #A3 and $\pm 4\%$ for those velocities calculated between accelerometers #A1 and #A4. These figures are based on the assumption that the depth measurements are accurate to ± 0.1 inch and the time measurements are accurate to ± 0.05 milliseconds; these figures are quite conservative for the ruler used to measure depth and the oscilloscope time base used to measure time delay between pulses. It is readily apparent that as the depth between accelerometers increases from accelerometer #A1, the measured distance tolerance becomes less and less significant, thus increasing the accuracy

TABLE II. Sound Velocities, Builder's Sand

Test Number	Frequency, KHz	Calculated Velocities, ft/sec		
		#A1 to #A2	#A1 to #A3	#A1 to #A4
1	10.0	573	535	565
	3.0	573	535	565
	1.6	573	535	565
2	10.0	417	471	
	3.0	521	507	557
	1.6	573	535	565
3	10.0	546	525	555
	3.0	533	507	555
	1.6	573	525	555
4	10.0	509	525	576
	3.0	573	545	583
	1.6	573	560	583
5	10.0	509	525	576
	3.0	546	535	576
	1.6	603	560	590
6	10.0	539	535	574
	3.0	539	547	574
	1.6	611	560	592
7	10.0	573	547	583
	3.0	539	547	574
	1.6	628	560	583
8	10.0	611	574	592
	3.0	539	552	583
	1.6	655	560	583
9	10.0	533	542	570
	3.0	521	535	574
	1.6	611	552	583
10	10.0	552	542	565
	3.0	552	547	574
	1.6	611	560	574
11	10.0	573	547	574
	3.0	539	535	570
	1.6	611	547	574
12	10.0	573	560	592
	3.0	553	560	588
	1.6	655	588	602

of the calculated velocity. With these tolerances in mind, the sound velocity through sand is 583 ft/sec \pm 24 ft/sec. There is also no apparent increase/decrease in velocity due to moisture content. Hardin¹ and Paterson² have observed that sound velocity decreases as the moisture content increases. Their experiments, however, were conducted with a confining stress applied to sand samples. Their velocity calculations are also higher than the calculated velocities listed in Table II. However, as they point out, velocity increases as the confining stress increases. Since the tube tests were conducted on sand under no confining stress other than its own weight, the velocities obtained do not seem unreasonable. Hardin explains that the stiffness of the frame (sand) is reduced by the presence of moisture and is thus responsible for a decrease in the velocity of propagation. Again, his tests were conducted on sand under a uniform confining stress. Since we are simulating near surface behavior, the sand's frame stiffness is already low. The effects of moisture on the frame stiffness should therefore be much less, and consequently, the effect on velocity should therefore be much less. In any case, within the limits of experimental accuracy, neither the moisture content in the sand nor the driving frequency exhibit any effect on the sound propagation velocity.

Since the wavelength of sound within the sand medium is our primary concern for imaging purposes, Table III lists the wavelengths calculated assuming a sound velocity of 583 \pm 24 ft/sec. The equation used is

$$C = \lambda f \quad (2.1.1)$$

where C = sound velocity
 λ = wavelength
f = frequency

TABLE III. Wavelengths of Sound in Sand

Frequency KHz	Wavelength, λ inches
10.0	0.7
3.0	2.3 \pm 0.1
1.6	4.4 \pm 0.2

For the purpose of obtaining a reflected signal from a buried mine, a large ratio of object dimension to wavelength is desired. As this ratio increases from one, so does the possibility of resolving the mine's boundaries and thus its shape. From Equation (2.1.1) we note that for a given frequency, the wavelength is directly proportional to the velocity of sound in the medium. Thus, the velocity of sound in the medium determines how low a probing frequency we may use and still maintain a high enough object dimension-wavelength ratio to discern the shape of the object. Table III indicates, for the sound velocities thus far measured in sand, a frequency as low as 1.6 KHz may be utilized and still resolve the shape of the object.

Since the attenuation of sound in soil increases with frequency, the lower the probing frequency the greater the probing depth below the soil's surface (for a given power input to the sound projecting transducer). Table IV lists the attenuation data obtained from the tube tests in sand.

The tube test data led to qualitative information about the interaction between sound probing frequency, attenuation and moisture content for a given type of soil. The attenuation tests on sand indicate the following:

1. As expected, the attenuation of sound increases as the probing frequency increases.
2. The attenuation between accelerometers #A1 and #A2 appears to be very much affected by moisture content. In test number 2, as water is first added to the dry sand, the signal levels at these top two accelerometers rapidly rises, the attenuation between them rapidly decreasing. This is due to the fact that as water fills the pore spaces, the impedance between the moist sand and the water cell above are more closely matched. Better coupling of the transmitted signal at the boundary is then possible. As the moisture content becomes more evenly distributed, the increase in mass due to the water begins to attenuate the signal as it propagates down the tube.

TABLE IV. Calculated Attenuation, Builder's Sand

Test Number	Frequency KHz	Calculated Attenuation, dB/ir		
		#A1 to #A2	#A1 to #A3	#A1 to #A4
1	1.6	-0.86	-0.74	-0.58
2		-1.61	-0.85	-0.81
3		-0.33	-0.40	-0.32
4		+0.23	-0.35	-0.33
5		-0.33	-0.38	-0.40
6		-0.11	-0.24	-0.26
7		-0.14	-0.57	-0.47
8		-0.1	-0.74	-0.60
9		-0.42	-0.69	-0.48
10		-0.49	-1.03	-0.86
11		-0.71	-0.88	-0.86
12		-0.64	-0.65	-0.44
1	3.0	-2.56	-1.01	-0.83
2		-0.13	-0.85	-0.68
3		-0.5	-1.15	-0.95
4		-0.25	-0.37	-0.63
5		-0.20	-0.62	-0.45
6		-0.43	-0.72	-0.69
7		-1.94	-1.35	-1.08
8		-1.91	-1.37	-1.09
9		-1.16	-1.07	-0.94
10		-2.0	-1.33	-1.5
11		-1.24	-1.17	-1.31
12		-2.64	-1.79	-1.46
1	10.0	*	*	*
2		-6.15	-4.73	-3.3
3		-7.98	-3.96	-3.04
4		-5.42	-3.96	-3.04
5		-8.28	-3.80	-3.11
6		-7.85	-4.26	-3.32
7		-6.64	-4.27	-3.67
8		-9.83	-4.68	-2.95
9		-8.48	-4.3	-3.25
10		-8.69	-4.37	-3.53
11		-6.99	-3.99	-3.23
12		-7.98	*	*
		-4.10	-3.11	-2.94

* Attenuation too severe to measure.

3. At the dry and evenly distributed moisture contents, the severest attenuation generally occurs near the surface. This is most likely the result of surface scattering³, the effect being less significant as the driving frequency decreases.
4. Figures 7 and 8 are graphs of the data in the last two columns of Table IV. The curves drawn through the data points are merely meant to show the general trend of the data as testing progressed. From these figures it appears that the least attenuation at all frequencies occurred during test numbers 3-6. From Table I, the moisture content during tests 4-6 was 3%; during test number 3, the moisture content within the top 5 inches was 4% and the water was seeping down. A moisture content of 4% seems to be as much as the sand can hold, if the sand is not constrained to hold a larger amount of water.
5. At 1.6 KHz the measured attenuations varied between 0.2 dB/inch and 1.0 dB/inch. At 3.0 KHz, the attenuation varied between 0.6 dB/inch and 1.8 dB/inch. At 10.0 KHz, the attenuation varied between 3.0 dB/inch and 4.8 dB/inch. If the signal travels 3 feet from transmitter-mine-receiver, the tube test results indicate the following worst case attenuations:
 - (1) at 1.6 KHz, 36 dB loss,
 - (2) at 3.0 KHz, 65 dB loss and
 - (3) at 10.0 KHz, 173 dB loss.

2.2 Tube Tests on Sand-Clay Mixture

The tube tests on a sand-clay mixture were conducted; however, because of the limited time available for these tests, the tests were limited to only a few conditions of moisture content. Table V lists the moisture contents within the tube; the moisture cell designations are those of Figure 3.

The soil moisture content was increased by uniform wetting of the top surface. The water was allowed to settle at least one day before conducting the series of velocity and attenuation tests. The wetting of the soil caused the soil to settle. The accelerometers thus moved further and

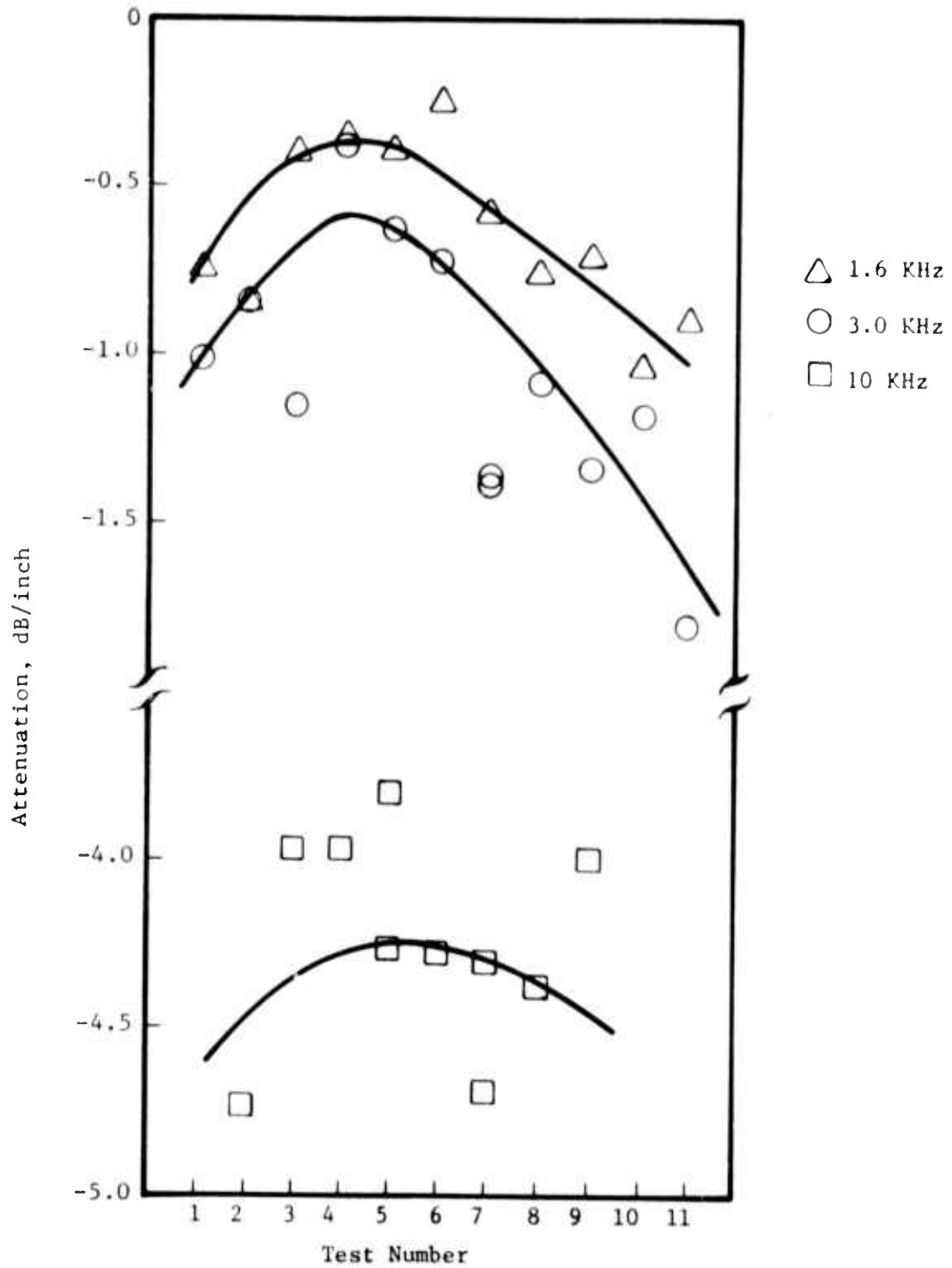


Figure 7: Attenuation between accelerometers #A1 and #A3 versus test number.

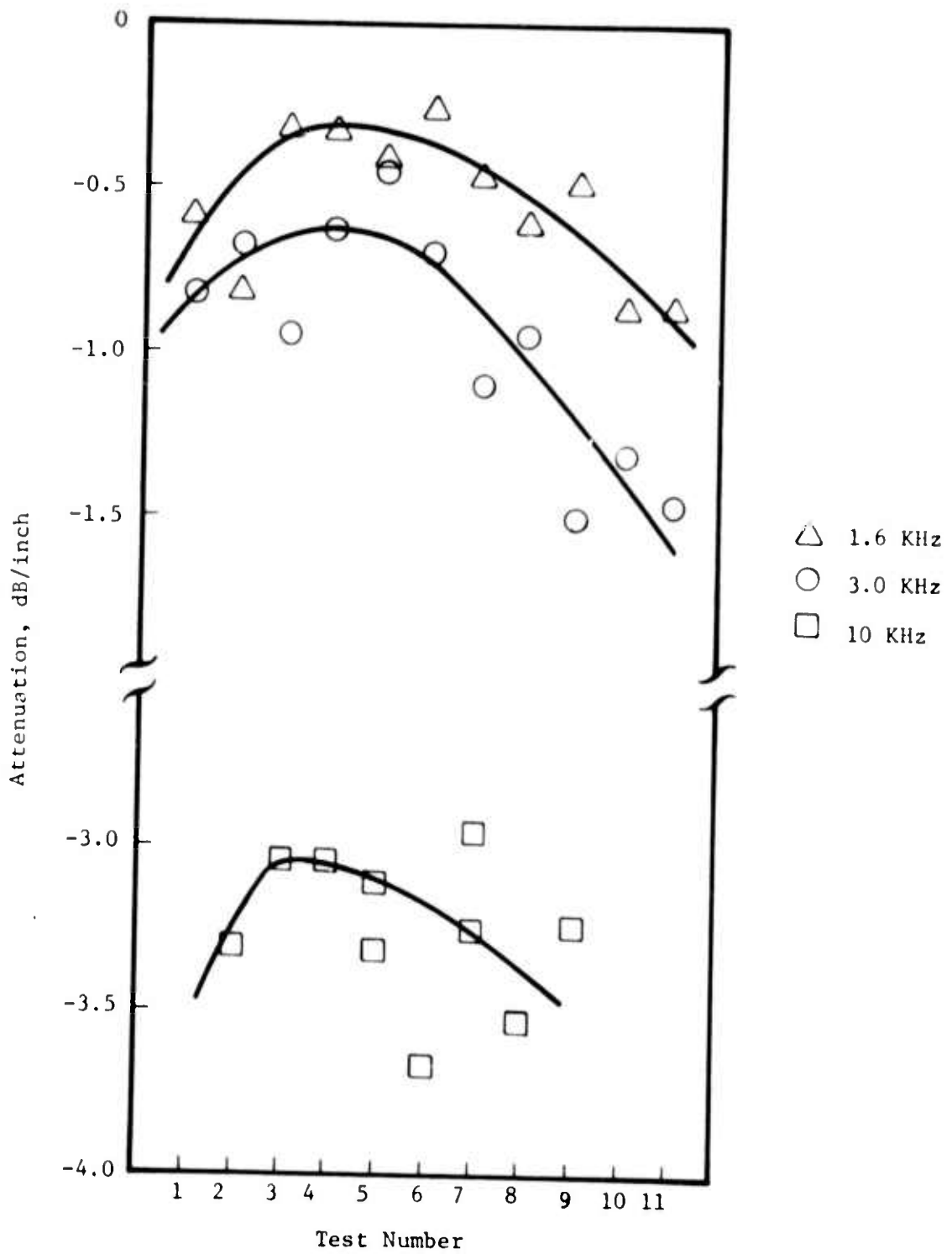


Figure 8: Attenuation between accelerometers #A1 and #A4 versus test number.

TABLE V. Moisture Content, Sand-Clay Mixture

Test Number	Moisture Content, % Water by Weight		
	#M1	#M2	#M3
1	0	0	0
2	0	0	0
3	0	0	0
4	8	8	7
5	8	8	7
6	8	8	7
7	8	8	7
8	9	10	8
9	9	11	9
10	9	11	9

further down with each wetting. This situation was not appreciated until test number 9 had been completed. For this reason, the relative position of the accelerometers is not known for tests #4 thru #9. For the dry-soil test and final test (#10) the positions of the accelerometers are known. Valid velocity calculations can, therefore, only be made for tests #1, 2, 3, and 10. Attenuation can be determined if the three bottom accelerometers are referenced to the top accelerometer. Since the relative position of the accelerometers is not known (other than those specified) the attenuation loss per inch cannot be calculated.

Had the settling of the soil been realized earlier, no obvious methods are available to determine exact relative accelerometer placement. Digging up and replacing the accelerometers with each wetting would have caused air to mix in with wet soil. This procedure would in itself negate the simulation of rain falling on a naturally existing sandy-clay soil.

Due to this occurrence of soil settling, only the results of tests considered valid and characteristic of the soil are presented. Table VI lists the velocities calculated and Table VII lists the attenuation losses calculated.

TABLE VI. Sound Velocity, Sand-Clay Mixture

Test Number	Voltage Input Volts, Peak to Peak	Frequency KHz	Sound Velocity Feet per Second		
			A1-A2	A1-A3	A1-A4
1-3	300	10	460	456	476
	400		473	465	476
	600		473	406	476
	100	3	460	448	466
	200		487	456	476
	200		447	737	471
	300		487	456	484
	400	1.6	487	456	476
	100		536	573	471
	200		487	469	476
100	3		958	829	844
200		902	829	866	
300		902	329	866	
400		902	829	866	
100		1.6	807	802	824
200			807	789	824
300			807	802	804

TABLE VII. Acoustic Attenuation, Sand-Clay Mixture

Test Number	Voltage Input Volts, Peak to Peak	Frequency KHz	Acoustic Attenuation Decibels Per Inch		
			A1-A2	A1-A3	A1-A4
1-3	300	10.0	-4.94	-3.96	-2.84
	400		-4.91	-4.11	-2.78
	600		-4.63	-4.20	-2.87
	100	3.0	-2.44	-2.60	-1.52
	200		-2.72	-2.63	-1.56
	200		-2.69	-2.66	-1.65
	300		-2.68	-2.50	-1.55
	400	1.6	-2.81	-2.45	-1.58
	100		-1.29	-1.98	-1.26
	200		-1.29	-1.96	-1.57
	200		-1.29	-1.96	-1.57
	10	100	3.0	-3.41	-2.81
200		-3.62		-2.96	-2.70
300		-3.70		-2.94	-2.83
400		-3.66		-2.90	-2.78
100		1.6	-1.08	-1.69	-1.80
200			-1.21	-1.81	-1.87
300			-1.49	-1.96	-1.87
300			-1.49	-1.96	-1.87

In the wet soil it was not possible to determine either velocity or attenuation of the 10 KHz signal. A low frequency response, as occurred in the pure sand tests, was apparent (i.e., the deeper accelerometers received only a low frequency subharmonic of the 10 KHz pulse). Since the attenuation of the 10 KHz signal was so severe and the low frequency subharmonic contained only a small portion of the input energy, no measurements could be made.

It appears that the velocity of propagation is a function of soil moisture content. There is a significant increase in velocity for a wet soil as opposed to a dry soil. The sound velocity has very little, if any, dependence on frequency. The attenuation losses appear to be greater in the sand-clay mixture as opposed to that obtained in a pure sand.

3.0 REFLECTION TESTS

The test site for experiments simulating in-situ conditions consists of a 30' x 30' x 12' tent around which a fence had been erected (Figure 9). Inside the tent, an 8' x 8' x 4' pit had been excavated and the walls of the pit lined with plywood sheets (Figure 10). The pit was filled with sand in layers about 2-3 inches thick. After each layer was added, the sand was uniformly compacted with a lawn roller and a tamping tool used to compact the sand around the edges. The sand was added to a depth of approximately 44 inches (Figure 11). Soil moisture cells were buried in the sand as indicated in Figure 12.

Since the sand in the pit was slightly different from that used in the tube tests, a sieve analysis was made of random samples. Figure 13 illustrates the particle size distribution for this sand.

As a preliminary investigation, prior to reflection tests, wave propagation in the pit sand was analyzed. Two accelerometers were buried in the center of the 8' x 8' x 4' pit. One accelerometer was buried at a depth of 6 inches and the other at a depth of 12 inches. A tube 18 inches high (24 inch inside diameter) was cut and lined with three sheets of plastic. One of the sheets was coated with a thin layer of tar. This tube, simulating the field deployable roller, was placed directly over the buried accelerometers. The tube was filled with water to a depth of 12 inches. One at a time the acoustic transducers were immersed in this water. The bottom surface of the transducer was placed 2 to 4 inches from the bottom. Figure 14 illustrates the instrumentation configuration utilized. The test set-up is similar to that used for the tube tests except that a wave analyzer and x-y chart recorder have been added. With this configuration it was possible to determine an amplitude frequency spectrum for the input signal to the transmitting transducer and also the amplitude frequency spectrum of any acoustic signals received by the buried accelerometers. Figures 15-23 are typical graphs of the frequency spectrums obtained.

The input signal was a repetitive burst of 16 cycles (at the transducer's resonant frequency) followed by a 128 cycle "off" period.

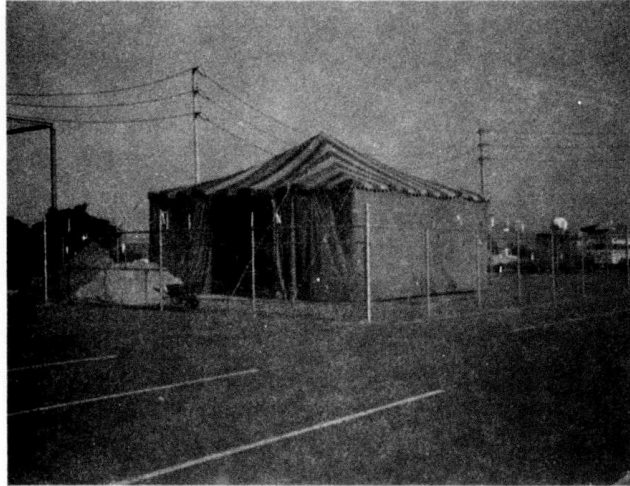


Figure 9: Tent covering area in which reflection tests were conducted.

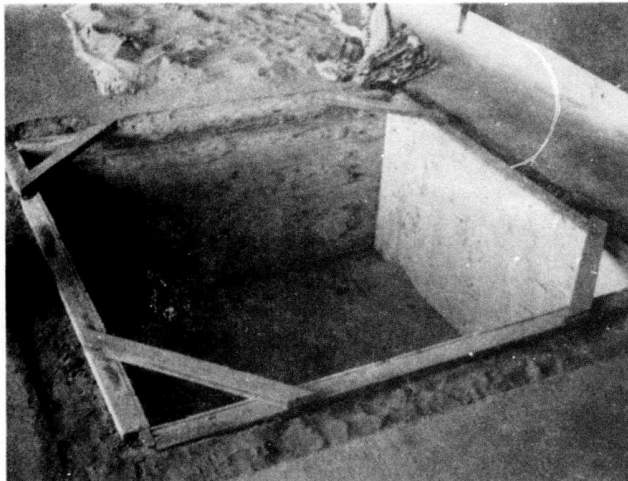


Figure 10: 8' x 8' x 4' pit.

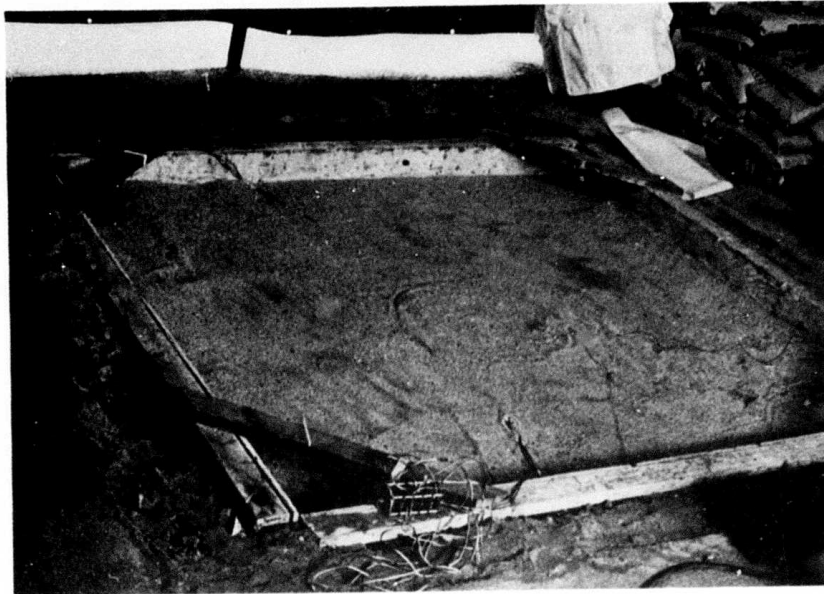


Figure 11: 8' x 8' x 4' deep pit. The pit has been filled with sand to a depth of approximately 44 inches.

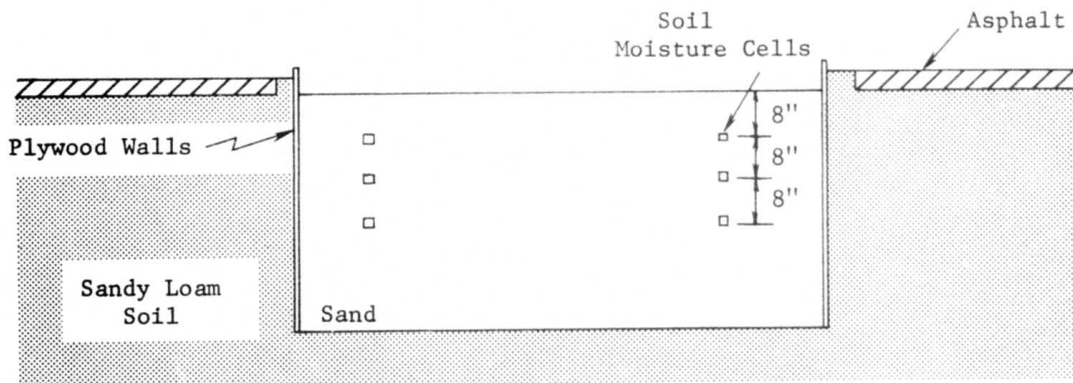


Figure 12: Cross-sectional representation of 8' x 8' x 4' pit filled with sand.

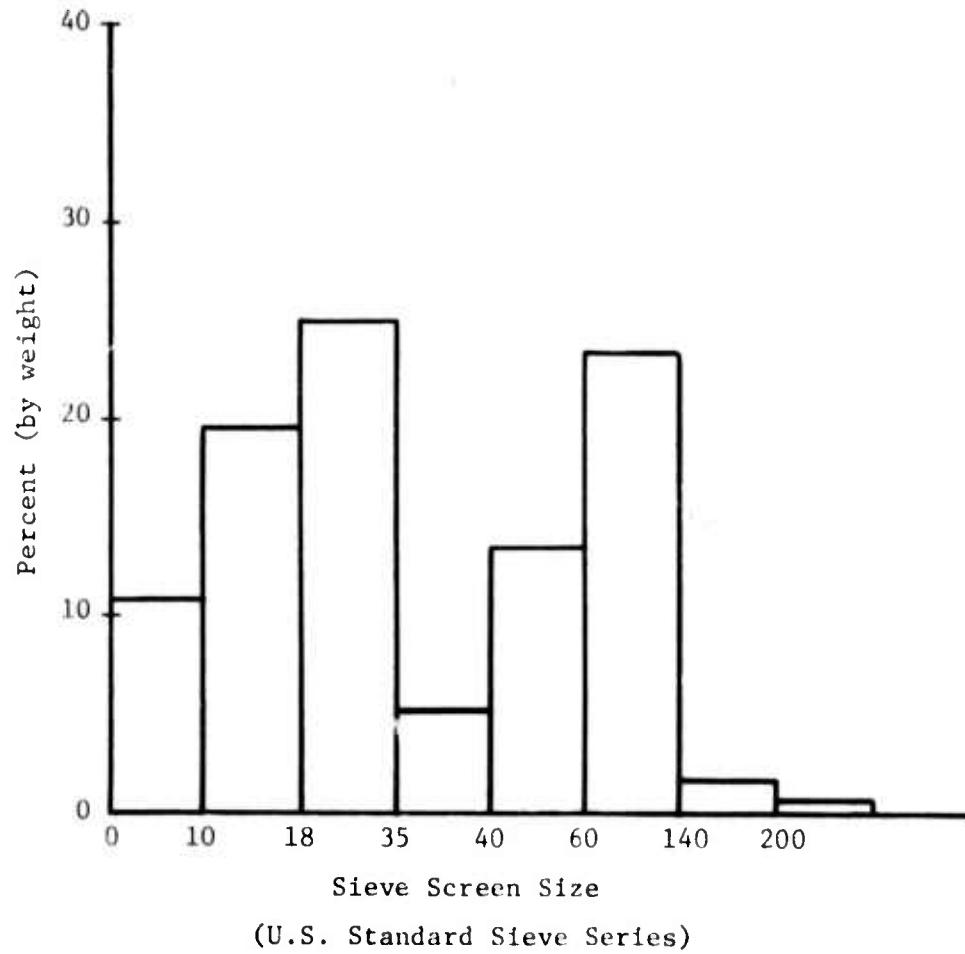


Figure 13: Particle size distribution for sand in large test pit.

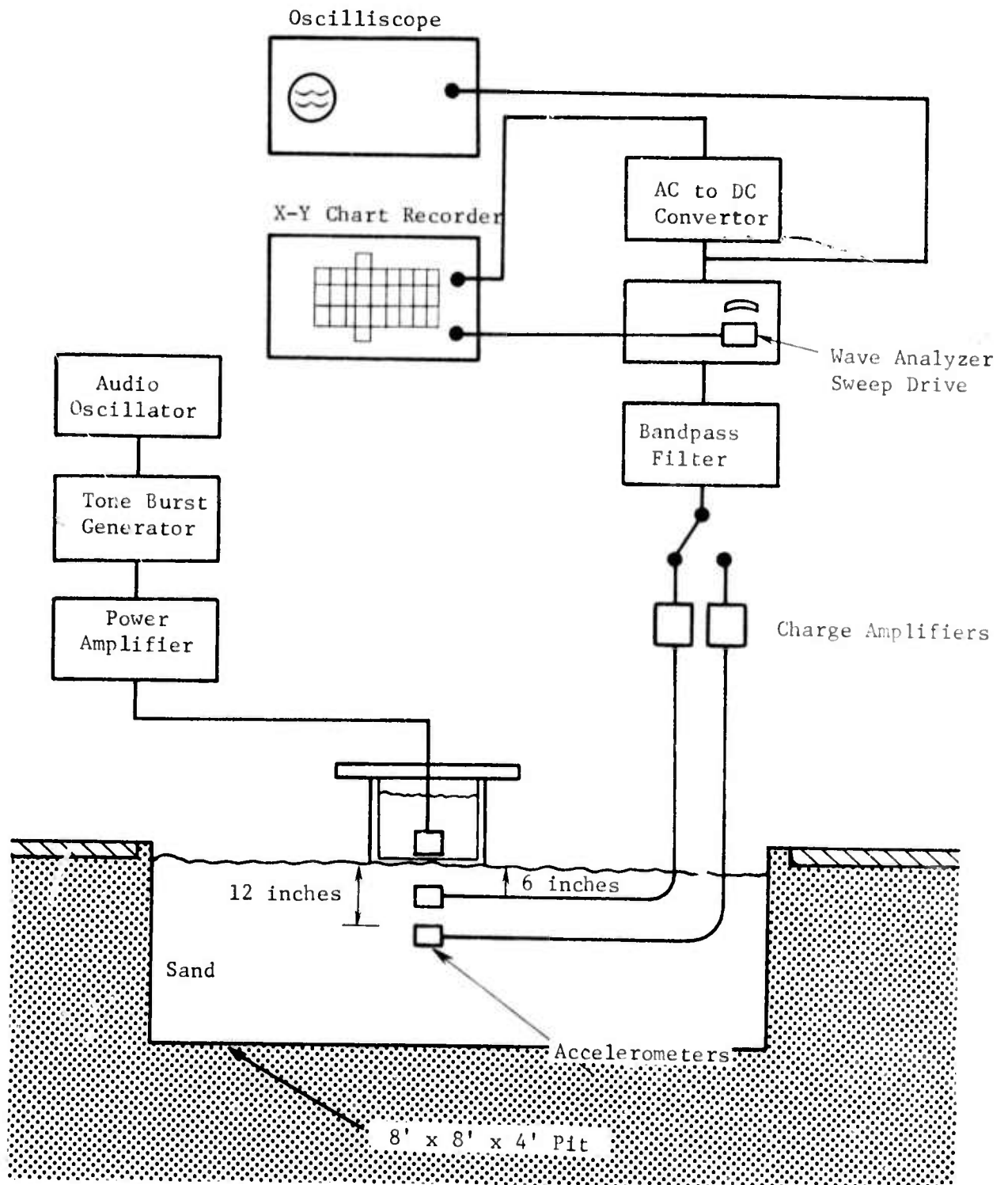


Figure 14: Instrumentation configuration.

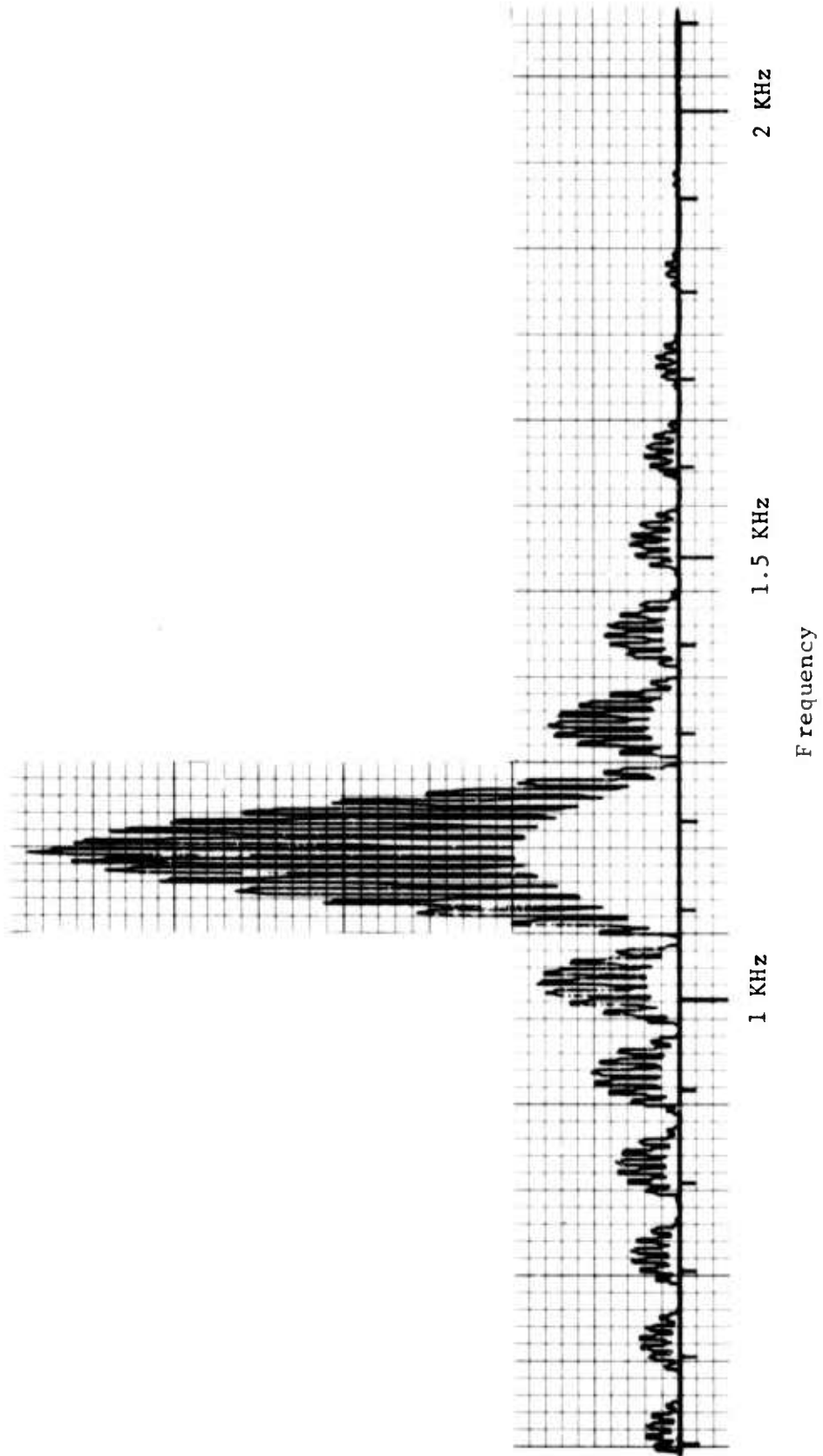


Figure 15: Frequency spectrum of input to 1.6 KHz transducer. Burst of 16 cycles on, 128 cycles off. Weighting factor: 0.9.

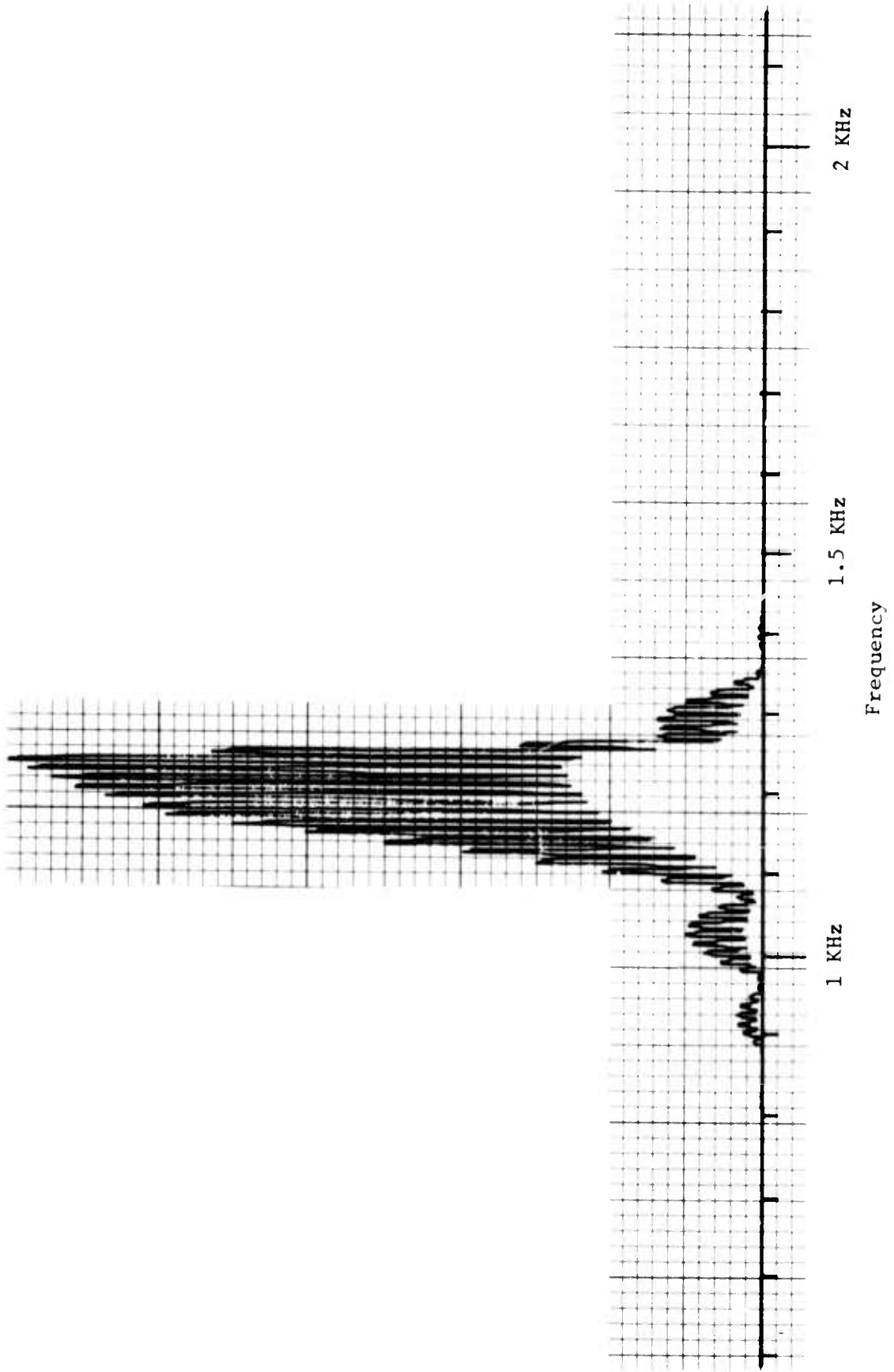


Figure 16: Frequency spectrum of response from 6 inch deep accelerometer. Weighting factor: 0.3.

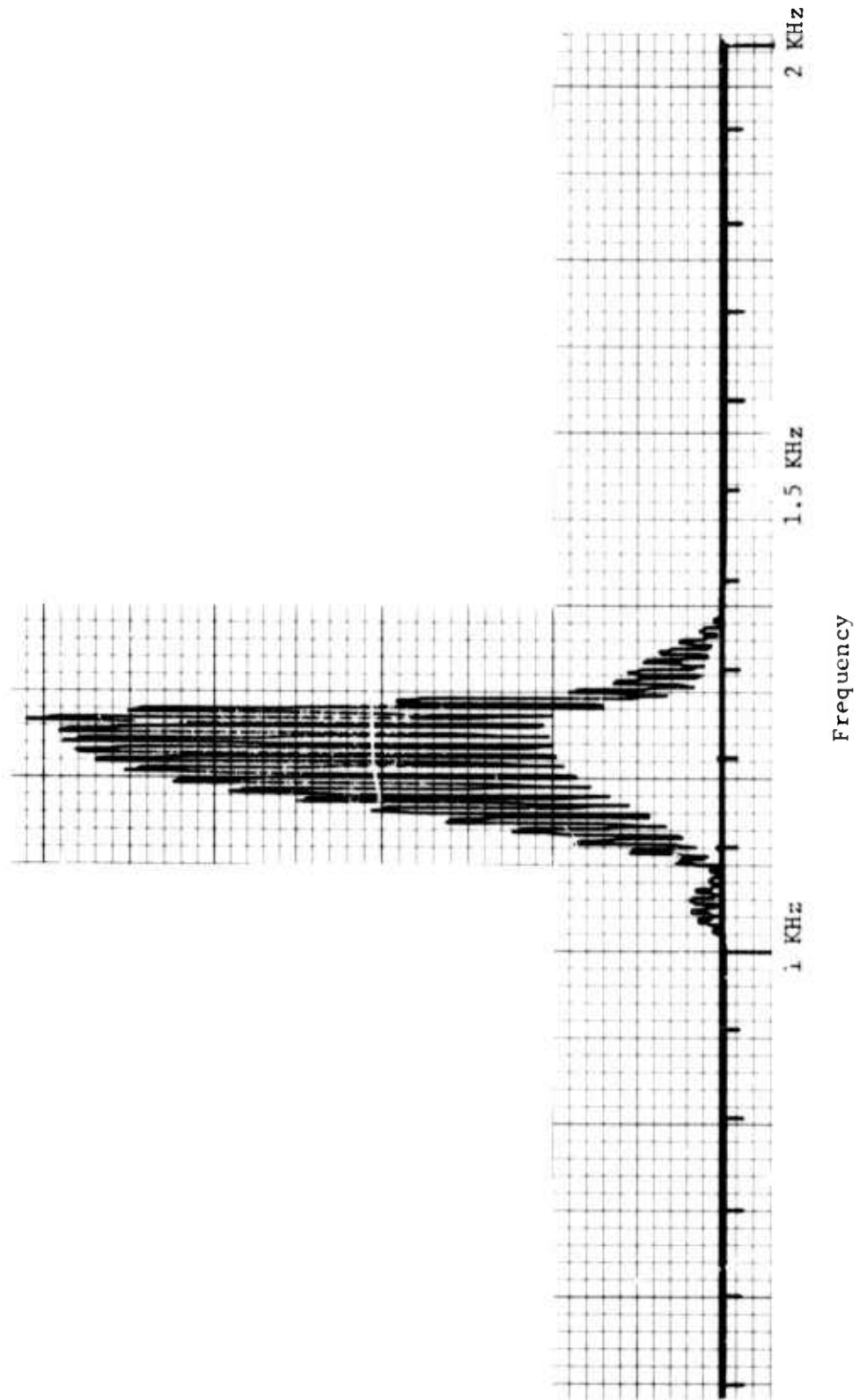


Figure 17: Frequency spectrum of response from 12 inch deep accelerometer. Weighting factor: 0.3.

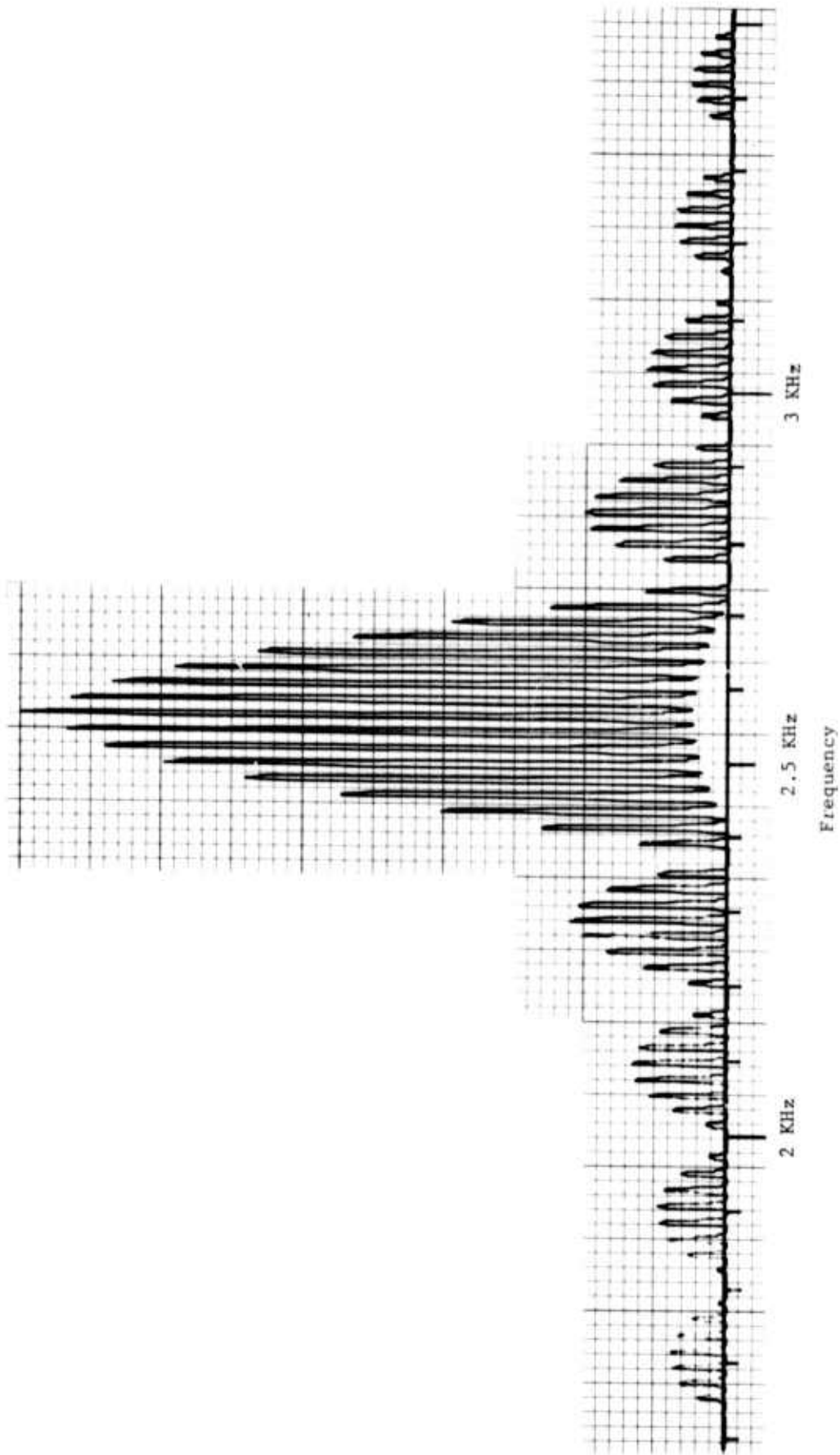


Figure 18: Frequency spectrum of input to 3 KHz transducer. Burst of 16 cycles on, 128 cycles off. Weighting factor: 3.0.

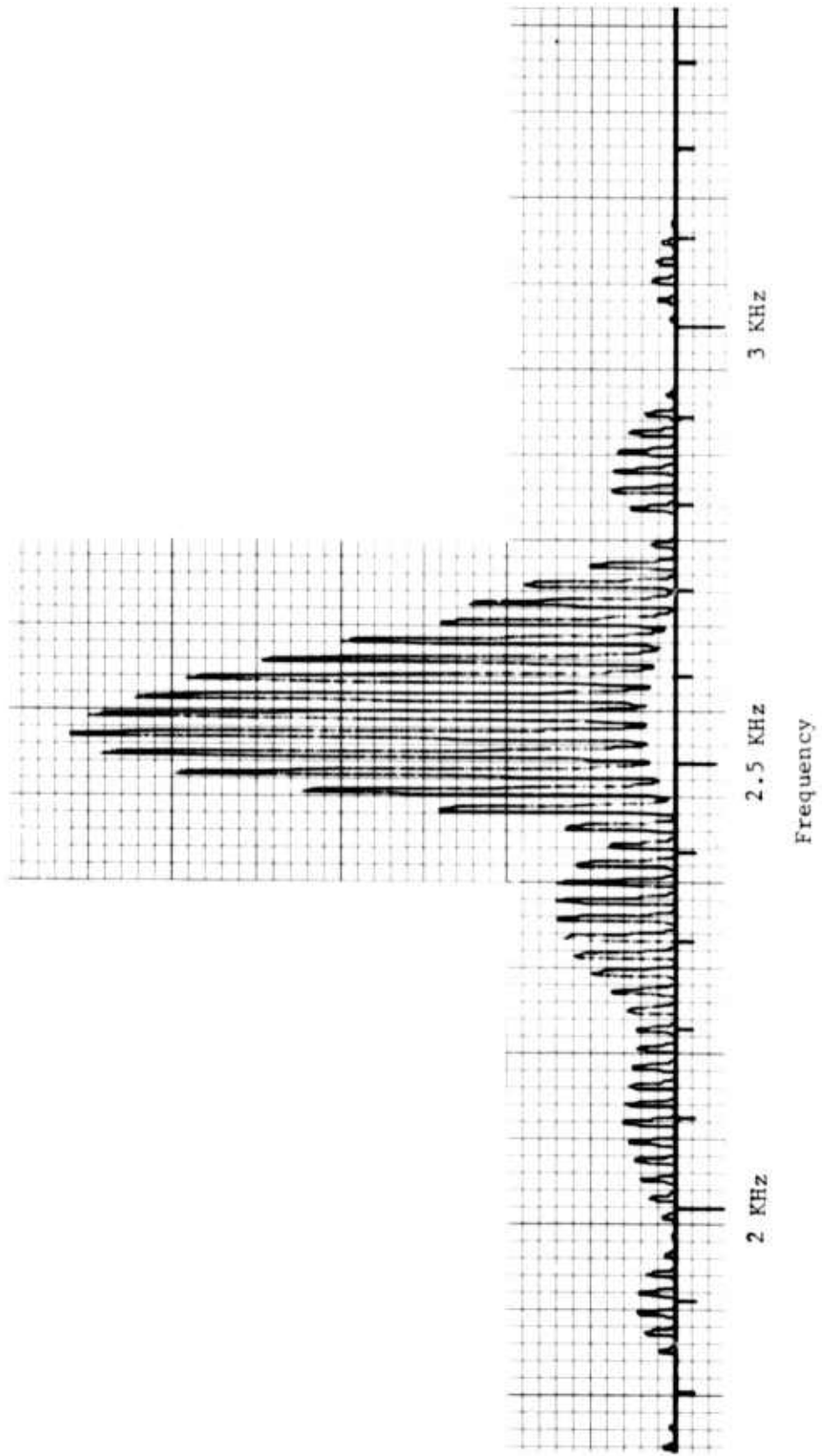


Figure 19: Frequency spectrum of response from 6 inch deep accelerometer. Weighting factor: 0.3.

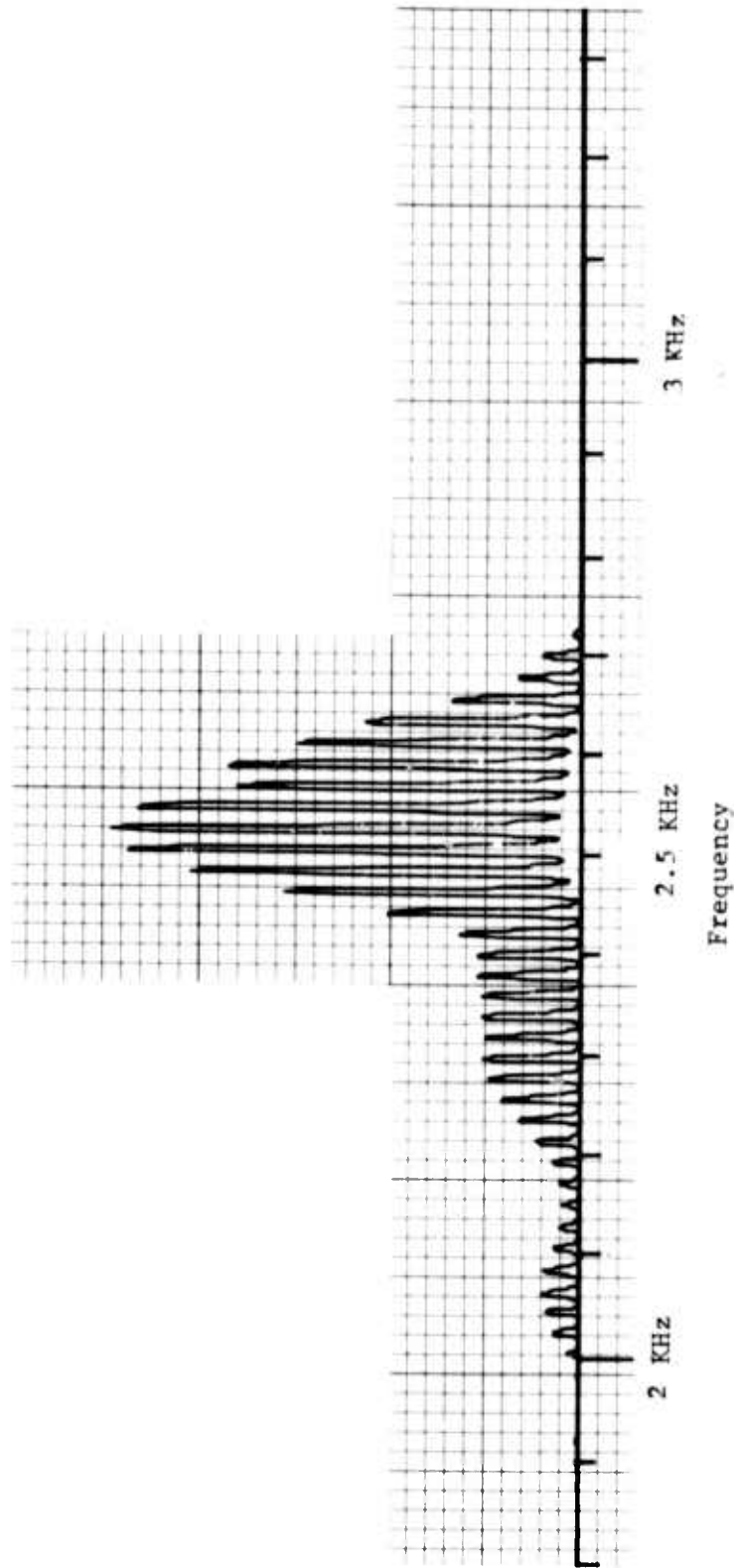


Figure 20: Frequency spectrum of response from 12 inch deep accelerometer.
Weighting factor: 0.3.

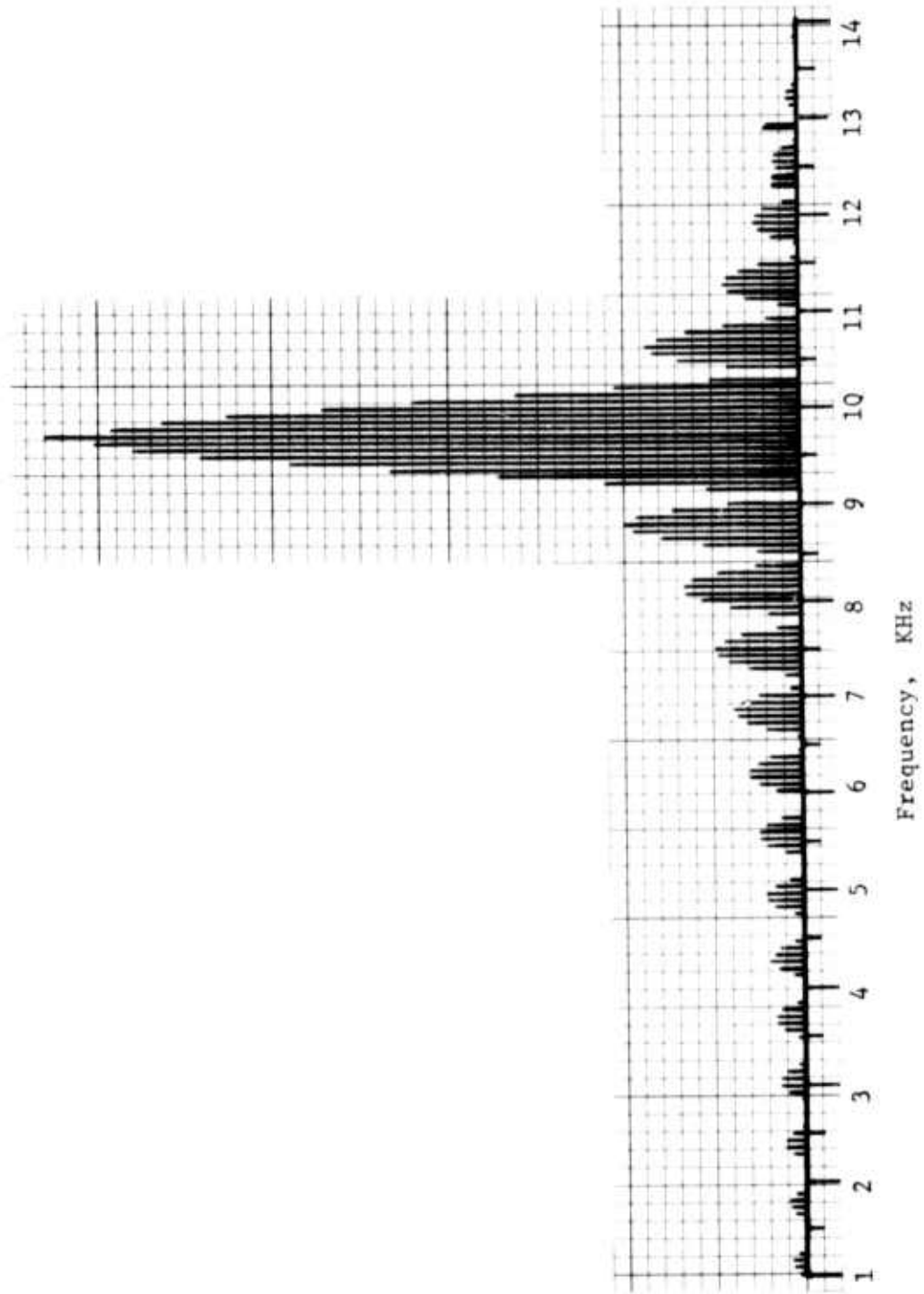


Figure 21: Frequency spectrum of input to 10 KHz transducer. Burst of 16 cycles on, 128 cycles off. Weighting factor: 3.0.

Figure 22: Frequency spectrum of response
from 6 inch deep accelerometer.
Weighting factor: 0.03.

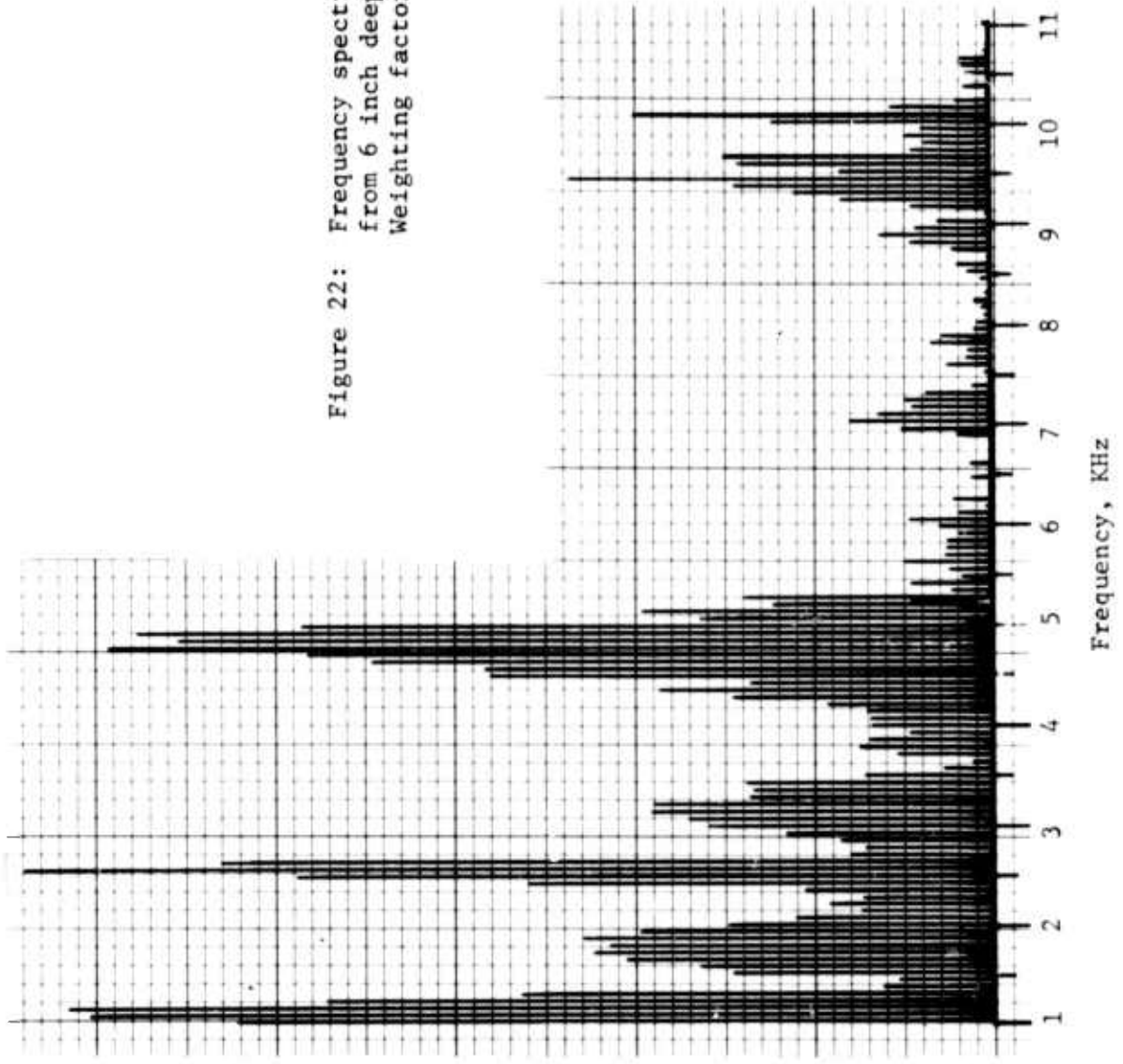
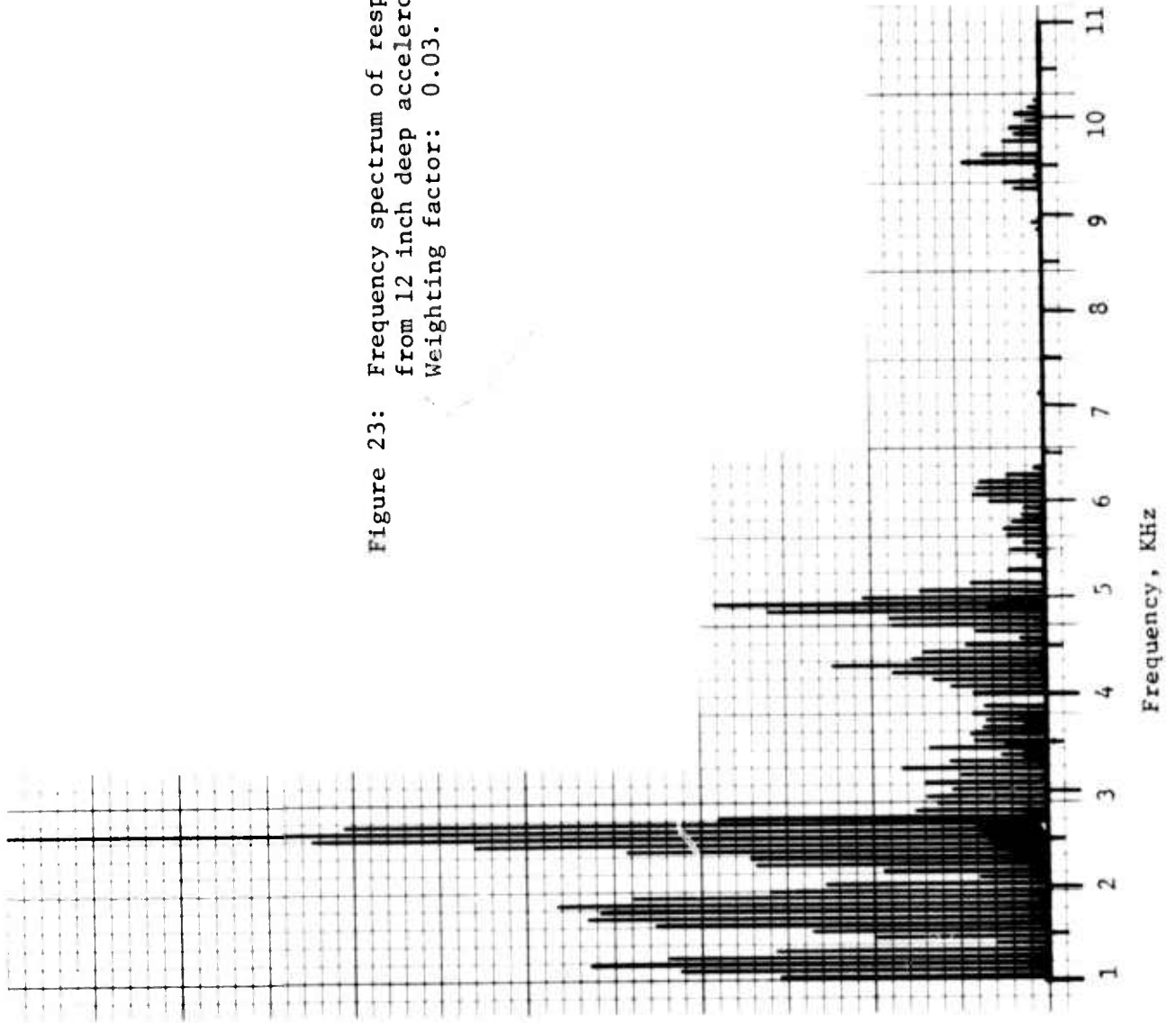


Figure 23: Frequency spectrum of response
from 12 inch deep accelerometer.
Weighting factor: 0.03.



The weighting factors listed on each figure indicate the relative amplitude or vertical scale of the graph. For each frequency, the same weighting scale is used for each accelerometer signal analysis.

Figures 15-17 illustrate the results of the 1.6 KHz test. Figure 15 is the frequency spectrum of the signal fed into the transmitting transducer. The center frequency is approximately 1.17 KHz. Figures 16 and 17 which are the accelerometer responses at the 6 and 12 inch depths respectively, indicate that the frequency of greatest amplitude is 1.23 KHz. The high and low frequency lobes have been almost completely attenuated.

Figures 18-20 illustrate the results of the 3 KHz test. Figure 18 is the frequency spectrum of the signal applied to the transmitting transducer. The center frequency is 2.53 KHz. Figures 19 and 20 are the responses of the 6 and 12 inch deep accelerometers, respectively. Again, the high and low frequency lobes are attenuated; however, much of the first low frequency side lobe is retained. The center frequency did not change.

Figures 21-23 illustrate the results of the 10 KHz investigation. Figure 21 is the frequency spectrum of the signal applied to the transmitting transducer. The center frequency is approximately 9.7 KHz. Figures 22 and 23 are the responses of the 6 and 12 inch deep accelerometers, respectively. Notice the complete distortion of the original spectrum. Most of the acoustic energy appears to have been transformed to a lower frequency range. The primary response seems to be at 2.6 KHz. This illustrates the sand's filtering action on the 10 KHz pulse bursts.

Figure 24 illustrates the accelerometer's responses to the 1.6 KHz signal, Figure 25 the response to the 3 KHz signal and Figure 26 the response to 10 KHz. Since the 1.6 KHz and 3 KHz signals retained enough of a distinctive shape, velocity measurements could be made in the same manner described for the tube tests. These velocities ranged from 670-700 feet per second. These are 15-20% higher than the mean velocity calculated from the tube tests. The moisture content in the sand during

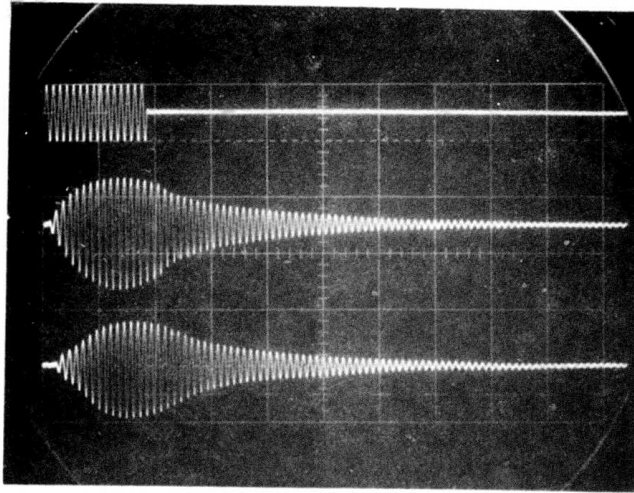


Figure 24: Response to burst of 16 cycles "on", 128 cycles "off" at 1.6 KHz. Top trace is proportional to input to transducer (scale: 5 v/division). Middle trace is response from 6 inch deep accelerometer (scale: 1 v/division). Bottom trace is response from 12 inch deep accelerometer (scale: 1 v/division). Horizontal scale: 5 msec/division.

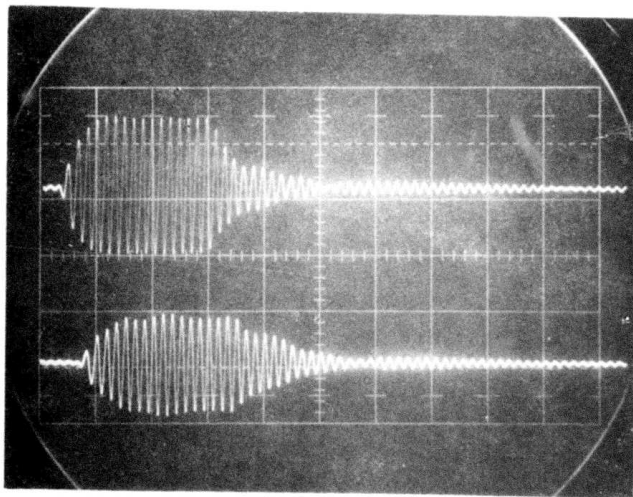


Figure 25: Response to burst of 16 cycles "on", 128 cycles "off" at 3 KHz. Top trace is response from 6 inch deep accelerometer (scale: .5 v/division). Bottom trace is response from 12 inch deep accelerometer (scale: .5 v/division). Horizontal scale: 2 msec/division.

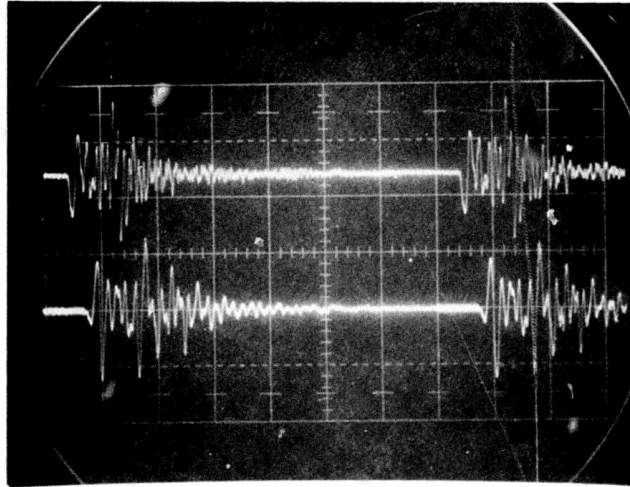


Figure 26: Response to burst of 16 cycles "on", 128 cycles "off" at 10 KHz. Top trace is response from 6 inch deep accelerometer (scale: 0.2 v/division). Bottom trace is response from 12 inch deep accelerometer (scale: 0.1 v/division). Horizontal scale: 2 msec/division.

these tests was 3%, 8 inches down, 7%, 16 inches down and 5%, 24 inches down. The top surface of the sand was fairly dry and loose.

3.1 Mine Reflection Tests

The objective of the mine reflection tests was to determine if an acoustic signal can propagate down to a metallic or non-metallic mine, reflect from the mine and return to the surface. The primary concern was whether or not the return signal would be of sufficient intensity to be picked up by the receiver and be distinguishable from surface waves which might obscure the return signal. In each of the mine reflection tests, a significant return signal was received and it was easily distinguishable from the surface waves.

Figure 27 illustrates the acoustic transmitting and receiving transducers utilized. Figure 28 illustrates the instrumentation necessary to generate and receive the acoustic signals. The acoustic transducers were immersed in water filled tubes which were lined with

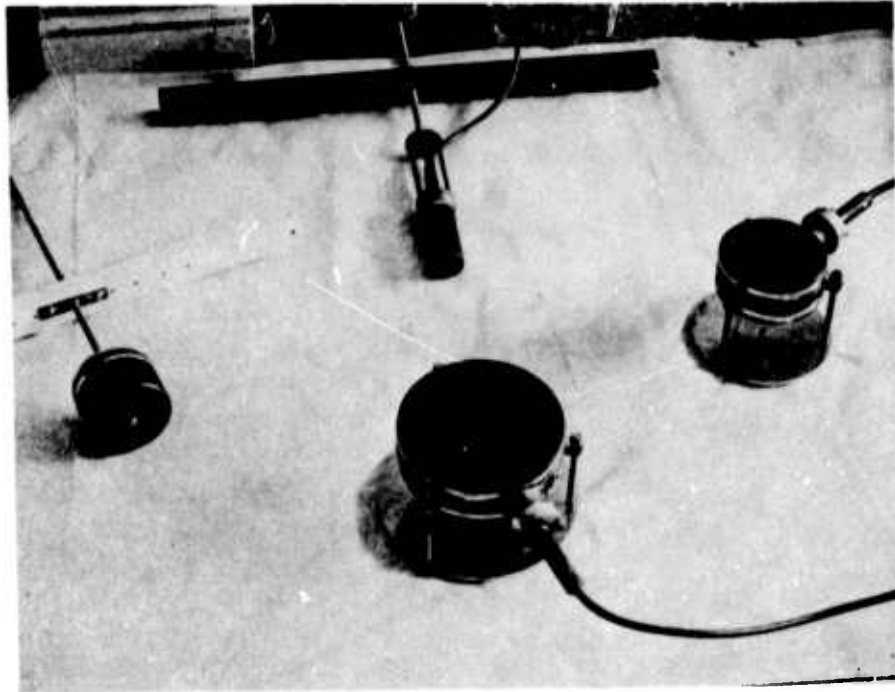


Figure 27: Transducers. From left to right, 10 KHz transmitter, 1.6 KHz transmitter (bottom), receiver (top) and 3.0 KHz transmitter.

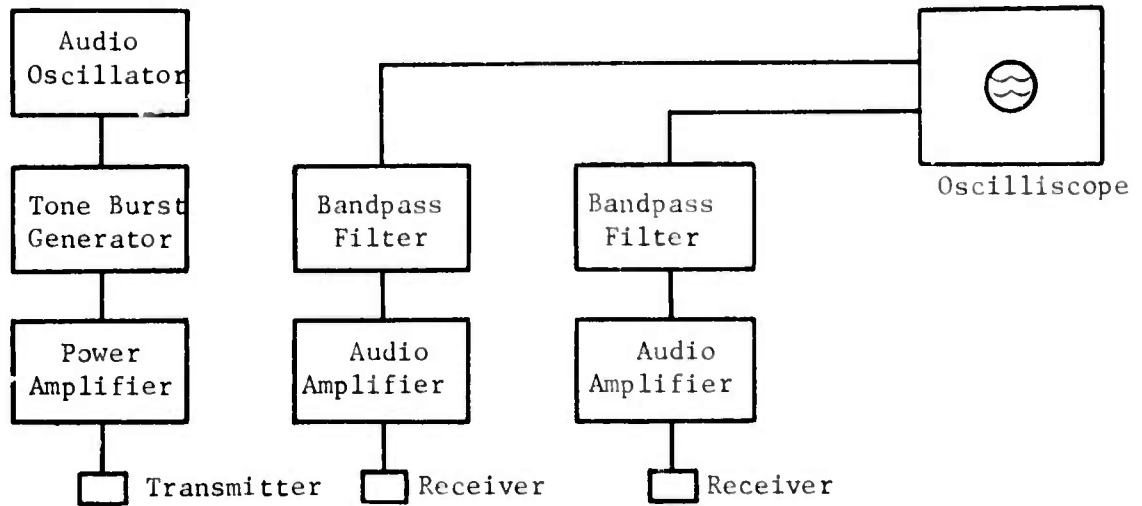


Figure 28: Instrumentation configuration for reflection testing.

four layers of plastic sheeting. The water serves as a coupling medium for propagating the sound into the soil. The reflection tests were conducted with the water filled tubes in different configurations (Figure 29). In Figure 29b, two tubes were placed directly over the buried mine, one for the transmitting transducer (T) and one for a receiving transducer (R_A). A third tube was placed, as indicated in the illustration, for receiving transducer (R_B). As Figure 29c illustrates, a mine was buried beneath two closely spaced water filled tubes. Three to four feet from these tubes another set of tubes were placed with the same separation distance; beneath these tubes, nothing was buried. The configuration of Figure 29a was used for more complete reflection tests and will be discussed later. It was the intent of each test layout to show a reflected signal from a buried mine and the type of signal received when no mine is present.

Figures 30-37 illustrate the objects used for reflection tests, they are (1) a simulated wooden mine, (2) a simulated steel mine using 1/16 inch steel plates, (3) a simulated steel mine using 1/4 inch steel plates, (4) a plastic block, (5) a simulated wax mine, (6) a small pocket of clay in sand to simulate a soil inhomogeneity, (7) a large rock, and (8) a small rock.

Reflection tests were made with the objects buried between six and twelve inches (measured from the ground surface to the top surface of the object). Initial tests utilized the tube arrangements of Figures 29b and 29c. Reflections were attempted with each of the three available frequencies, 1.6 KHz, 3.0 KHz and 10 KHz. Pulse bursts of 2 or 4 cycles "on" and 128 cycles "off" were used. Note that as far as the transmitter (T) and receiver (R_A) are concerned, there is no difference between the three configurations. The only difference is the method of showing what occurs when no mine is buried. In each case, the transmitter was placed close to the side of the tube and the receiver positioned for a maximum return pulse as displayed on the oscilloscope.

When the steel mine (1/4 inch plates) was buried (at a 9 inch depth) and the configuration of Figure 29c used, Figures 38-40 illustrate the reflected signals received at 10 KHz, 3 KHz and 1.6 KHz, respectively.

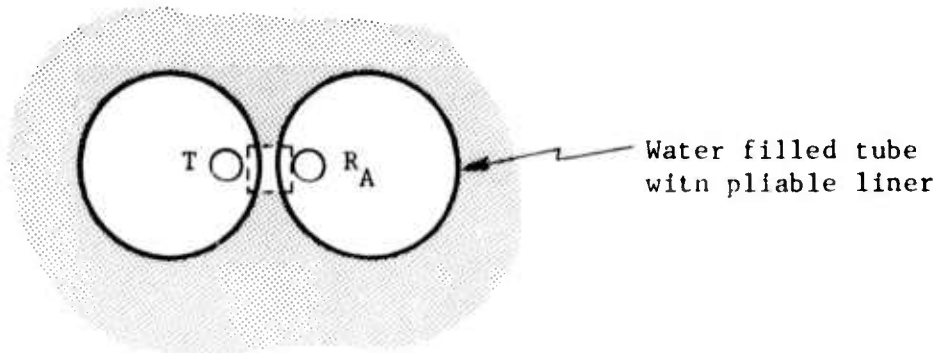


Figure 29a: Configuration I for reflection testing.

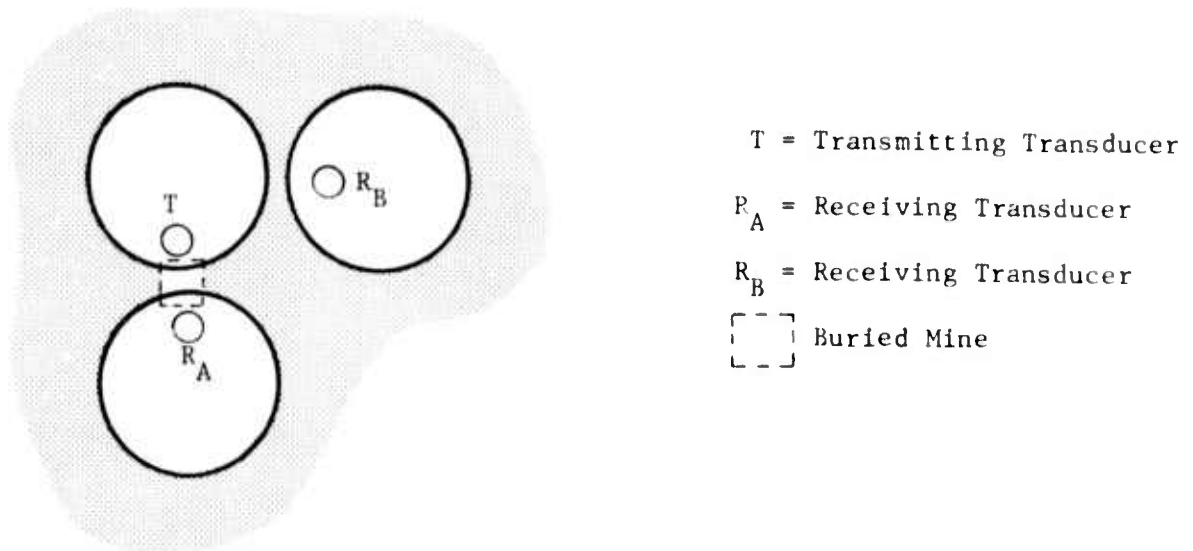


Figure 29b: Configuration II for reflection testing.

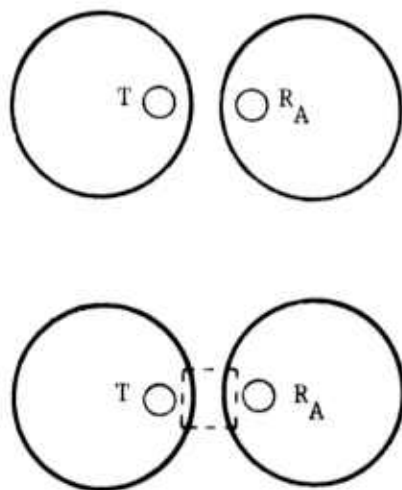


Figure 29c. Configuration III for reflection testing.

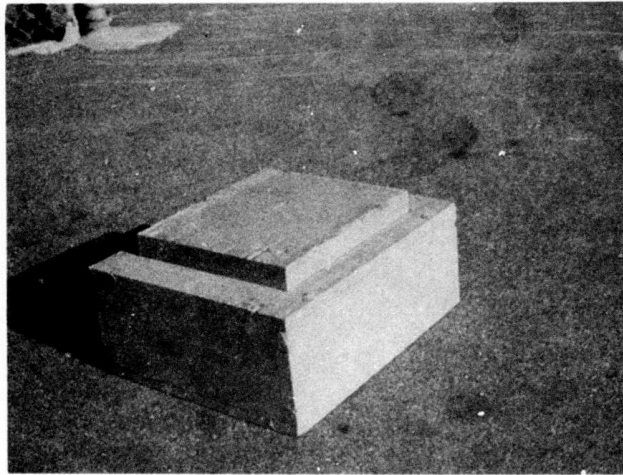


Figure 30: Simulated wooden mine, $12\text{-}5/8'' \times 10\text{-}1/2'' \times 6''$.

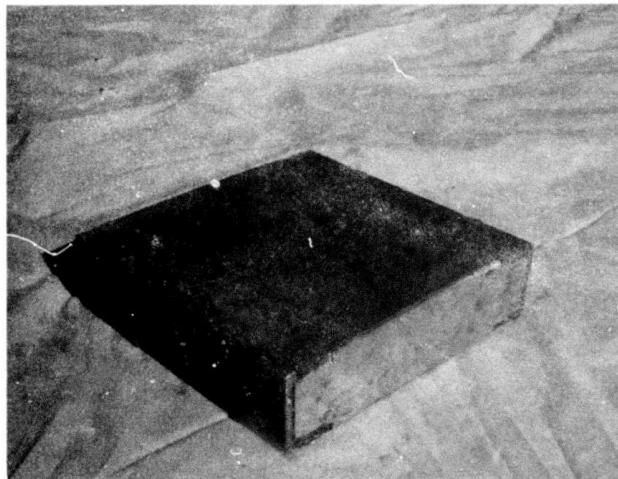


Figure 31: Simulated steel mine, $12'' \times 12'' \times 3/8''$. Top and bottom plates are $1/16''$ steel.



Figure 32: Simulated steel mine, 12" x 11-5/8" x 2-1/8". Top and bottom plates are 1/4" steel.

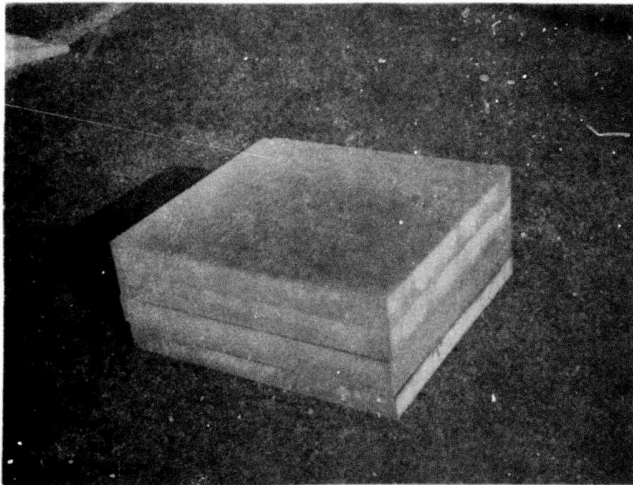


Figure 33: Plastic block 12" x 11" x 5".

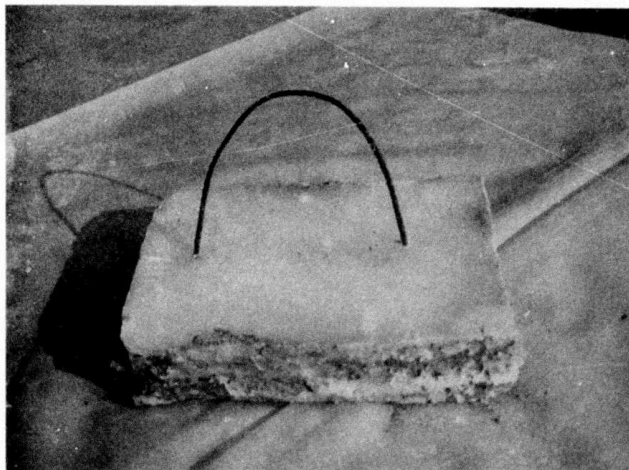


Figure 34: Simulated wax mine, 13" x 10-1/2" x 3". Wax was poured into a sand mold.

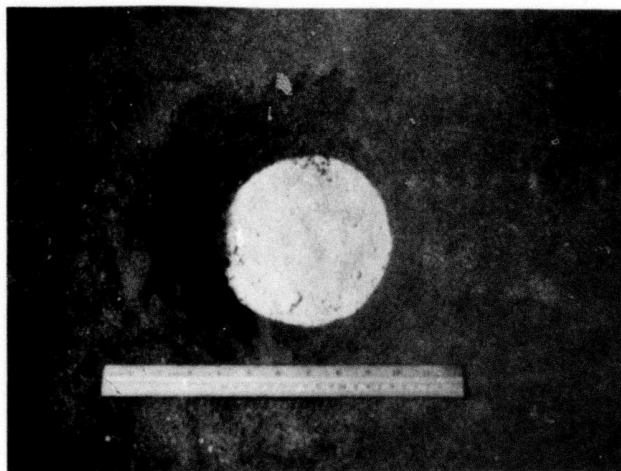


Figure 35: Simulated soil inhomogeneity. A clay pocket, 6" dia. x 4" deep, was buried in sand 6" below the surface.



Figure 36: Large rock used for reflection tests, approximately 9-1/2" x 8" x 8-1/2".



Figure 37: Small rock used for reflection tests, approximately 8" x 5" x 5".

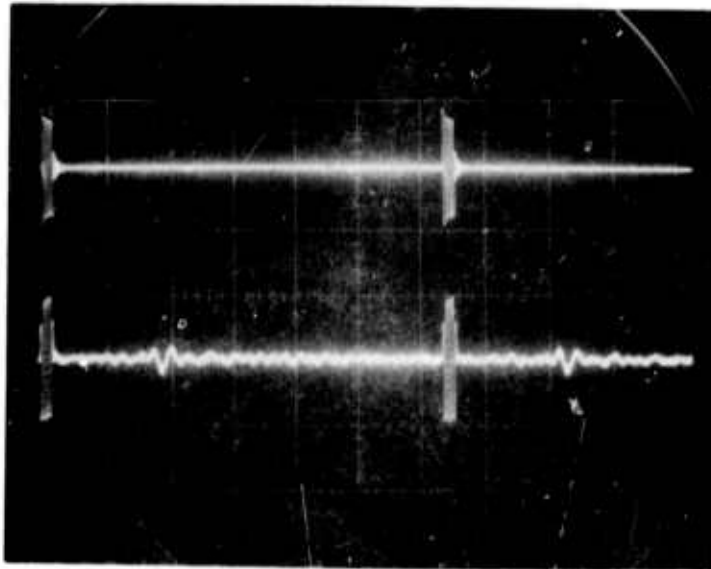


Figure 38: Reflection: Steel plate, 10 KHz. Top trace: 20 v/division, approximately 1/40 of input voltage to transmitter. Bottom trace: 0.05 v/division, reflection from 9 inch deep steel plate. Horizontal scale: 2 msec/division.

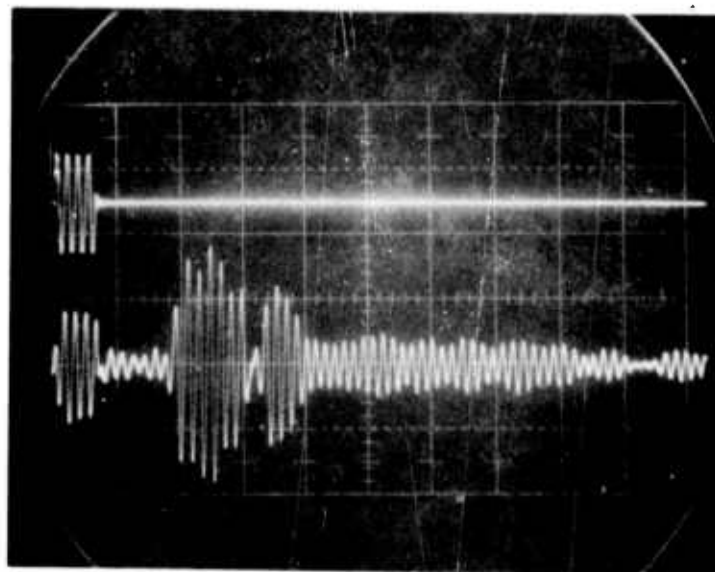


Figure 39: Reflection: Steel plate, 3 KHz. Top trace: 20 v/division, approximately 1/40 of input voltage to transmitter. Bottom trace: 0.05 v/division, reflection from 9 inch deep steel plate. Horizontal scale: 2 msec/division.

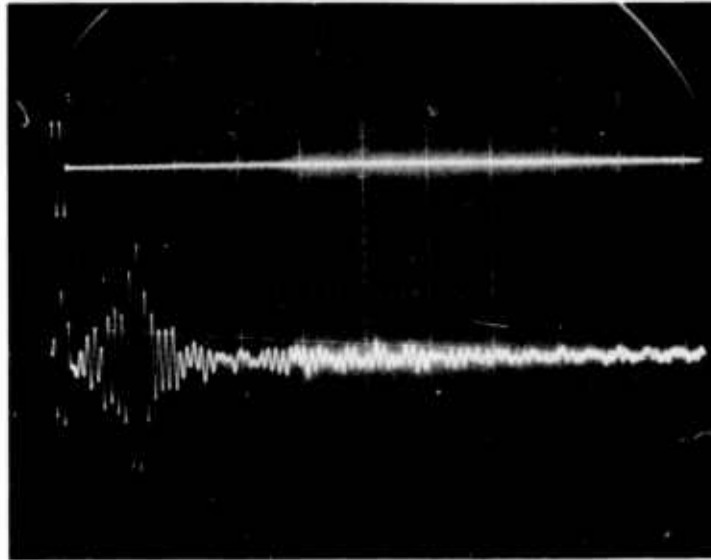


Figure 40: Reflection: Steel plate, 1.6 KHz. Top trace: 20 v/division, approximately 1/40 of input voltage to transmitter. Bottom trace: 0.05 v/division, reflection from 9 inch deep steel plate. Horizontal scale: 5 msec/division.

In each of these figures, the top trace illustrates the waveform fed into the transmitting transducer (T). The bottom waveform illustrates the amplified response of the receiving transducer (R_A). The 10 KHz reflected signal is a low frequency wave as previous accelerometer measurements predicted. The 3 KHz return signal appears to be composed of two pulses. The 1.6 KHz return signal appears to have signals both in front of and behind the primary 2 cycle information carrying signal. A two cycle burst was used for the 1.6 KHz frequency because of the larger period of each cycle. If a longer pulse burst was used, the return signal would display more overlapping of signals than those obtained with the 2 cycle pulse burst.

Figures 41-43 illustrate the reflected signals received from a buried (9 inch depth) wooden mine. No reflected signal could be detected using a frequency of 10 KHz. At 3 KHz, we again see two return pulses. The 1.6 KHz reflected signal does not have any clearly discernible pulse shape.

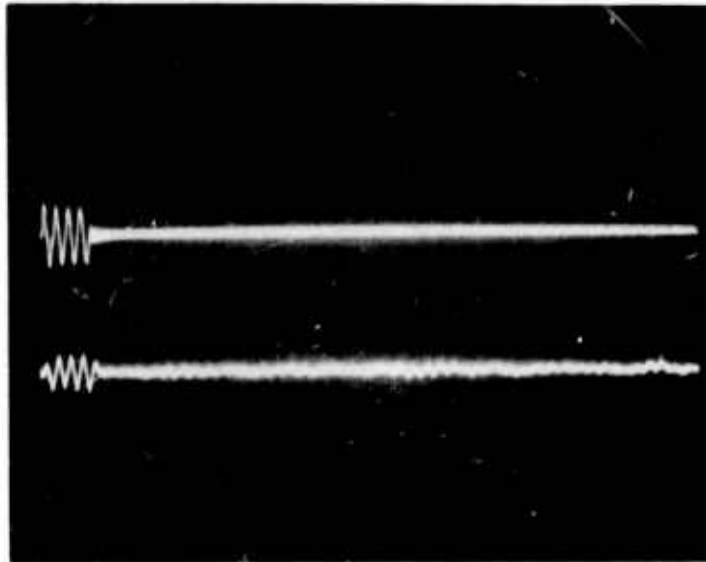


Figure 41: Reflection: Wooden mine, 10 KHz. Top trace: 1000 v/division, input to transmitter. Bottom trace: 0.02 v/division, receiver output. Horizontal scale: 0.5 msec/division.

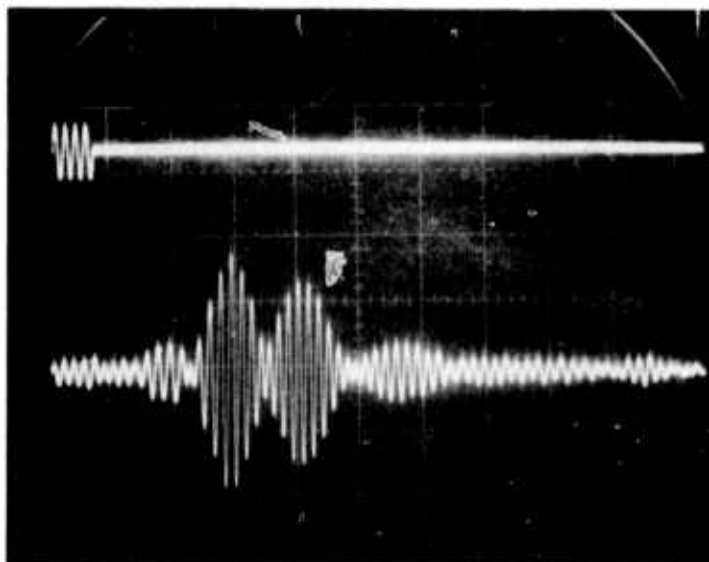


Figure 42: Reflection: Wooden mine, 3 KHz. Top trace: 1000 v/division, input to transmitter. Bottom trace: 0.02 v/division, receiver (R_A) output. Horizontal scale: 2 msec/division.

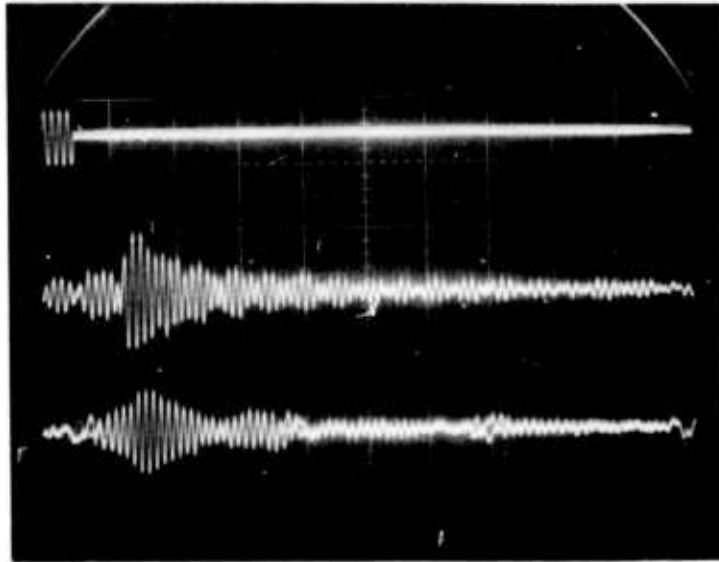


Figure 43: Reflection: Wooden mine, 1.6 KHz. Top trace: 1000 v/division, input to transmitter. Middle trace: 0.05 v/division, receiver R_A output. Bottom trace: 0.05 v/division, receiver R_B output. Horizontal scale: 5 msec/division.

The reflected 3 KHz signal from a buried plastic block (9 inch depth) is illustrated in Figure 44. The 10 KHz reflected signal was much like that for the steel plate. The 1.6 KHz reflected signal was like that received from the wooden mine.

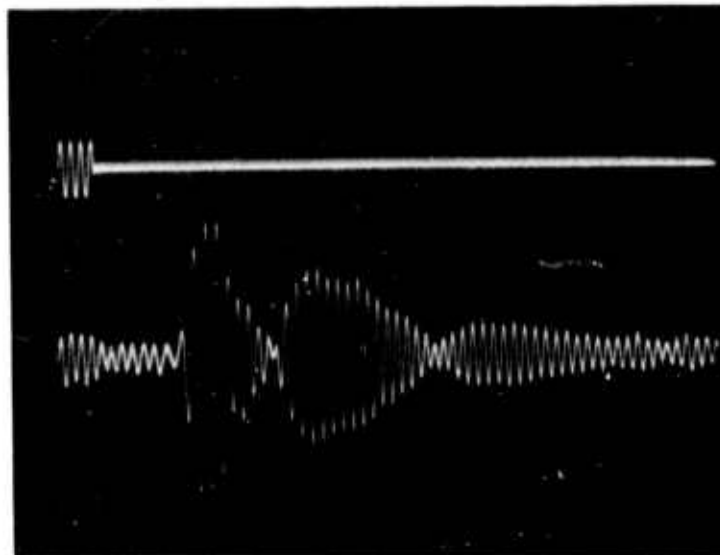


Figure 44: Reflection: Plastic block, 3 KHz. Top trace: 1000 v/division input to transmitter. Bottom trace: 0.02 v/division receiver output. Horizontal scale: 2 msec/division.

Regardless of the mine's composition, the following observations were made:

- 1) The reflected 10 KHz pulse was changed to a lower frequency as previous accelerometer tests indicated.
- 2) The signals received from the 1.6 KHz pulse are too cluttered to enable a reliable signal interpretation.
- 3) The 3 KHz pulse led to an easily discerned reflected pulse.
- 4) The received 3 KHz signals had two or three major pulse groups.
- 5) There was a small area within the received tube where the reflected signal was a maximum. The photographs were made in the area of maximum reception.

Since the use of the 3 KHz frequency apparently yielded the most discernible signal, further testing was done with only this frequency. In order to gain more information of the reflection signal the test configuration of Figure 29a was used. Realizing that the velocity of sound propagation will depend on compaction, accelerometers were buried in the sand along with the test objects. Figure 45 is a cross-sectional representation of the test configuration. After an object was emplaced, the fill soil was compacted in three layers. An accelerometer was placed at the bottom of each layer. A plumb line was used to position the accelerometers to ensure that they were on the same vertical axis. The depth of each accelerometer and the distance to the ground surface was measured from a fixed beam placed over the pit. The accelerometers were placed on an axis 3-4 inches from the mine's edge. Two water filled tubes were placed directly over the mine. The transmitter was placed in the tube above the accelerometers and positioned for maximum pulse signals at the accelerometers. The signals from the accelerometers were displayed on an oscilloscope and the arrival time of the pulses measured. Figure 46 illustrates the types of signals received. The time measurements were made on an expanded scale. These signals were obtained during tests on a wooden mine buried 12 inches. Since the depth of each accelerometer was known, the velocity in the soil could be calculated. The receiver was placed in the other tube and positioned for a maximum pulse reflection from the mine. Figure 47 illustrates the signal received during tests of a wooden mine

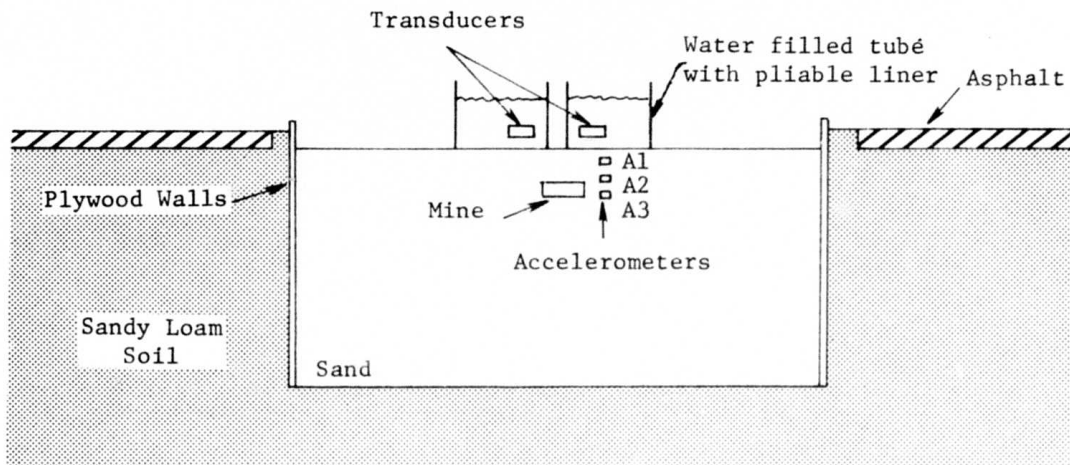


Figure 45: Cross-sectional representation of reflection test configuration utilizing accelerometers.

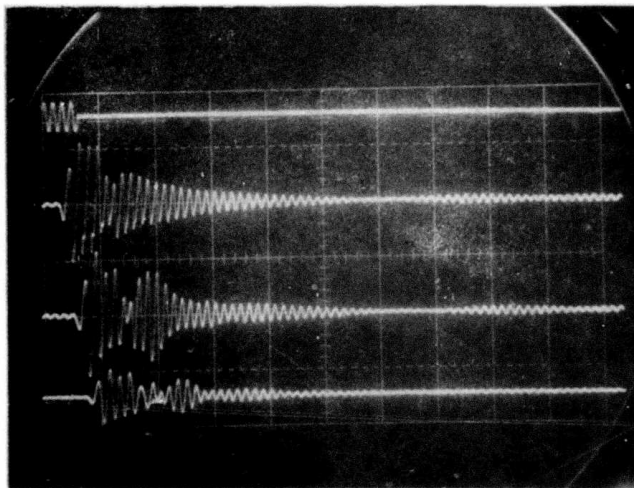


Figure 46: Traces from accelerometers. From top to bottom the traces are (1) input to transmitter, 2000 v/division; (2) accelerometer A1, 1.0 v/division; (3) accelerometer A2, 0.5 v/division; and (4) accelerometer A3, 0.5 v/division. Horizontal scale: 2 msec/division.

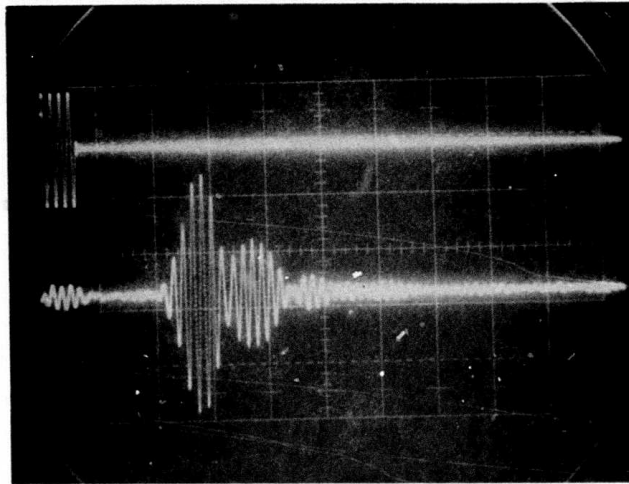


Figure 47: Reflected signal from wooden mine at a depth of 12 inches. Top trace is input to the transmitter, 500 v/division. Bottom trace is receiver output, 0.05 v/division. Horizontal scale: 2 msec/division.

buried 12 inches. This procedure was for determining the sound velocity and not for maximizing a mine reflection signal. The position of the transducers was measured. Assuming a linear wave propagation path, the distance traveled by a pulse signal (from transmitter to mine to receiver) can be estimated. Using the calculated velocity one can determine when the reflected signal should arrive. This estimated time of arrival can then be compared to the actual return pulses received.

The transmitting and receiving transducers were then interchanged from their respective tubes. The transmitter was then aligned for maximum signals at the bottom accelerometers. Figure 48 illustrates an example of the accelerometer responses during a wooden mine test. The receiver was then aligned for a maximum reception of the mine reflected signal. Figure 49 illustrates the signal received from a wooden mine. The arrival time of this reflected signal was measured on the oscilloscope. After measuring the position of the transducers, a linear wave path can be estimated and a predicted arrival time calculated. This predicted arrival time was then compared to the actual arrival time. Figures 50-55 illustrate

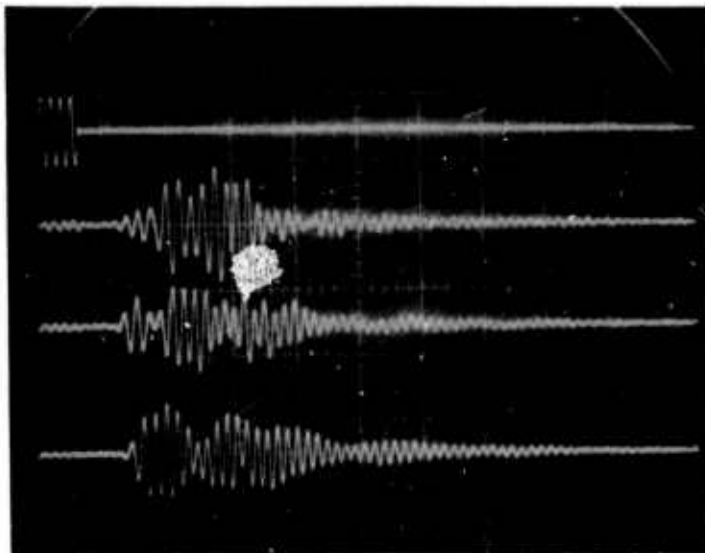


Figure 48: Traces from accelerometers. From top to bottom the traces are (1) input to transmitter, 1000 v/division; (2) accelerometer A1, 0.05 v/division; (3) accelerometer A2, 0.1 v/division; and (4) accelerometer A3, 0.1 v/division. Horizontal scale: 2 msec/division.

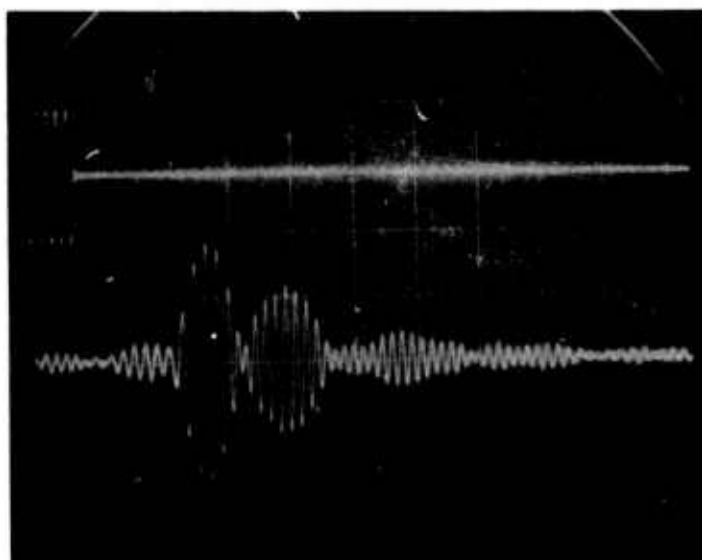


Figure 49: Reflected signal from a wooden mine at a 12-inch depth. Top trace is input to transmitter, 500 v/division. Bottom trace is receiver output, 0.05 v/division. Horizontal scale: 2 msec/division.

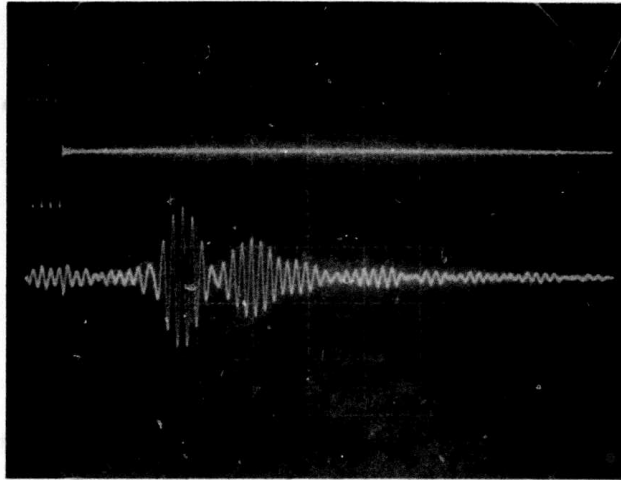


Figure 50: Reflected signal from plastic block at a depth of 12 inches. Top trace is input to transmitter, 500 v/division. Bottom trace is receiver output, 0.02 v/division. Horizontal scale: 2 msec/division.

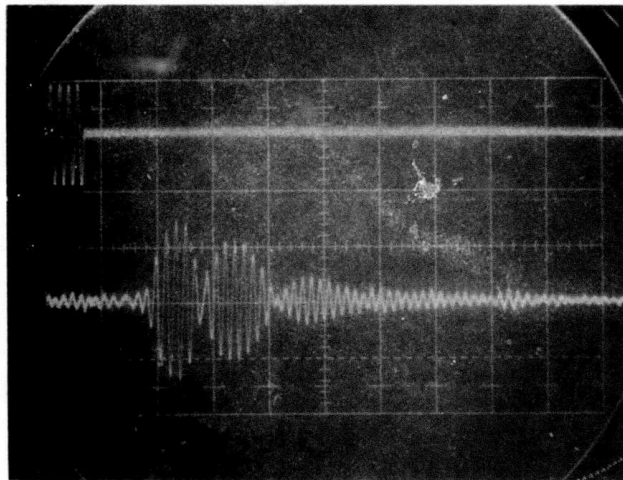


Figure 51: Reflected signal from steel mine with 1/4" plates at depth of 9 inches. Top trace is input to transmitter, 500 v/division. Bottom trace is receiver output, 0.02 v/division. Horizontal scale: 2 msec/division.

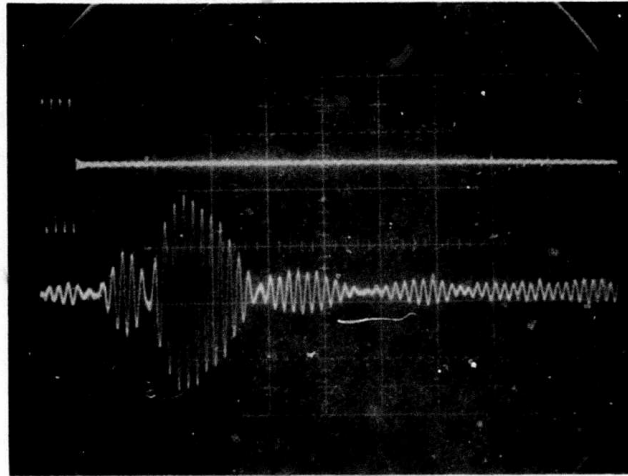


Figure 52: Reflected signal from a steel mine with 1/16-inch plates at a depth of 12 inches. Top trace is input to transmitter, 500 v/division. Bottom trace is received output, 0.02 v/division. Horizontal scale: 2 msec/division.

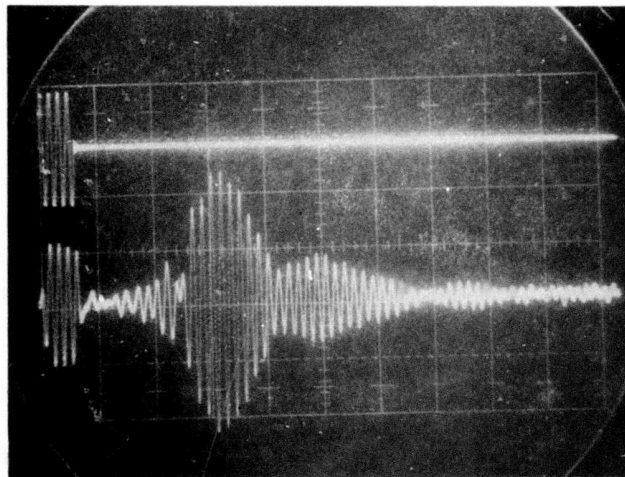


Figure 53: Reflected signal from a wax block at a depth of 11 inches. Top trace is input to transmitter, 500 v/division. Bottom trace is receiver output, 0.02 v/division. Horizontal scale: 2 msec/division.

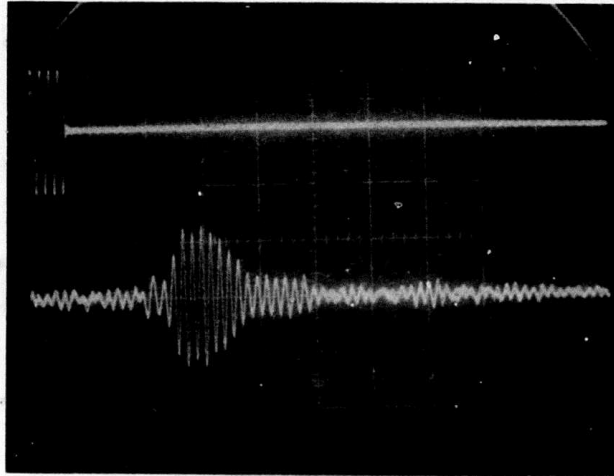


Figure 54: Reflected signal from large rock at a depth of 9 inches. Top trace, 500 v/division. Bottom trace is receiver output, 0.02 v/division. Horizontal scale: 2 msec/division.

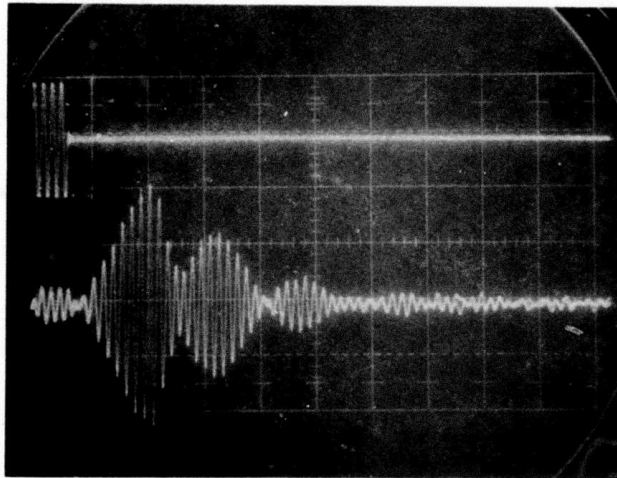


Figure 55: Reflected signal from small rock at a depth of 6 inches. Top trace, 500 v/division. Bottom trace is receiver output, 0.02 v/division. Horizontal scale: 2 msec/division.

the reflected signals received from the other objects. Figure 56 illustrates the signal received from a pocket of clay and Figure 57 illustrates the signal received with nothing buried below the transducers.

It is apparent from Figures 56 and 57 that there is no significant difference between the signals received from a homogeneous soil and the signals received when a small soil inhomogeneity is present. A small pulse is received which may be attributable to a surface wave. Since the placement of the tubes and transducers is about the same in each reflection test, one would expect this surface wave to appear in each trace of a mine reflection signal. In Figures 56 and 57 the surface wave arrived at the receiver between two and four milliseconds after the transmitted pulse. Indeed, in each of the mine reflection traces a small signal is present in this time range. The surface wave amplitude in these cases, however, is so minute that there is no possibility of mistaking it for a mine reflected signal. Apparently the energy contained in the reflect compressional wave dominates over the small longitudinal and transverse wave energies of the surface wave.

Table VIII summarizes the basic calculations and observations made during the reflection tests which utilized accelerometers. Realizing that wave propagation in a porous granular material is a very complex phenomenon, any attempt at quantifying wave behavior would at best be extremely difficult. Since the development of a mathematical model for acoustic wave propagation in soils was outside the scope and intent of the contract, the basic measurements made could only be used to demonstrate that the signals received are indeed reflected signals from mines. The predicted arrival times listed in Table VIII were calculated by (1) determining the total path traveled by a plane wave assuming an iso-velocity medium, and (2) dividing this path distance by the average sound velocity as calculated from the accelerometer signals. Refraction effects at the mine-soil boundary were neglected. Dispersion effects caused by the velocity gradient existing in the soil were neglected. Although these effects were neglected, the results are adequate enough to demonstrate that the first large pulse received in each reflection signal is indeed from the buried mine. Generally, the actual time of arrival was later than the predicted

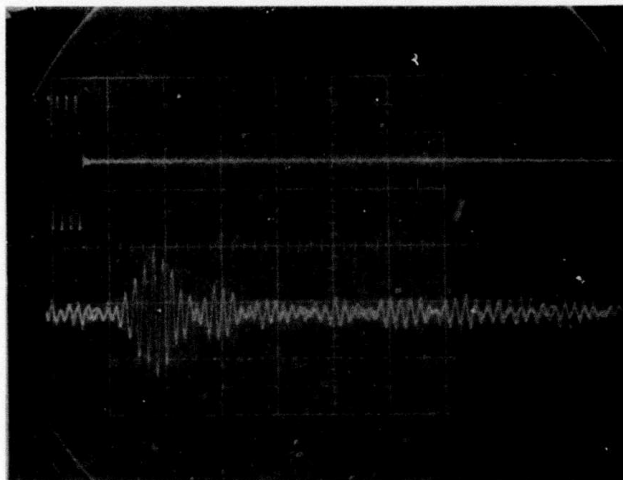


Figure 56: Reflected signal from pocket of clay at a depth of 6 inches. Top trace, 500 v/division. Bottom trace is receiver output, 0.02 v/division. Horizontal scale: 2 msec/division.

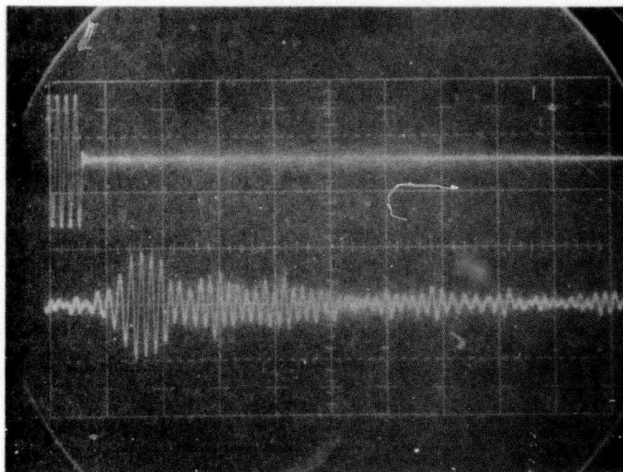


Figure 57: Signal received when nothing is buried. Top trace is input to transmitter, 500 v/division. Bottom trace is receiver output, 0.02 v/division. Horizontal scale: 2 msec/division.

TABLE VIII. Reflection Test Measurements

Object Material	Depth Inches	Velocity of Sound ft/sec	REFLECTION ARRIVAL CASE I		REFLECTION ARRIVAL CASE II	
			Actual msec	Predicted msec	Actual msec	Predicted msec
Wood	12	588	4.4	4.3	4.4	4.0
Wood*	7	515	3.8	3.9	3.3	3.2
Wax	11	588	5.2	4.2	5.0	3.8
Plastic	12	576	4.4	4.1	4.8	4.0
Plastic*	7	740	2.55	2.6	2.7	2.3
Steel ⁽¹⁾	9	606	3.5	3.2	3.5	3.2
Wax	6	690	3.0	3.1	3.2	2.8
Steel ⁽²⁾	12	641	4.0	3.8	5.1	3.9
Steel ⁽¹⁾	9	625	3.6	3.4	3.2	3.0

* Loose sand over mine

(1) 1/4-inch plates

(2) 1/16-inch plates

time of arrival, this may be due to neglecting both the ray bending effect occurring in a medium with a velocity gradient and also because refraction effects were neglected. The refraction effect is probably the primary reason that the actual and predicted times differ in Case II of Table VIII, also the velocity of sound in the soil may be somewhat irregular due to compaction.

There are generally two or three pulses discernible in the reflection traces. The first large pulse has been shown to be a reflection from the top surface of the mine. The second pulse does not appear to be from the back surface of the mine because the signals arrive later than would a back surface reflection. For the purposes of mine detection, the observed differences between the mine reflected signals and the signals received when no mine is present definitely indicate that acoustic waves can be used for detection of buried mines. Additional efforts would be required

to determine if the resolution is sufficient to be able to discern mines from naturally occurring objects. Tests conducted on rocks indicate that this would be possible. Irregularly shaped rocks tend to scatter the incident acoustic signal. Signals that are reflected occur along a particular axis of the rock; this axis and its existence depend both on the rock's orientation relative to the surface and also on its distribution of mass.

The soil moisture effect is evident by comparing Figures 51 and 58 which are the reflection traces from the steel mine with 1/4-inch top and bottom steel plates. Figure 51 was obtained at a soil moisture content of 3% whereas Figure 58 was obtained at a soil moisture content of approximately 7%. In the higher soil moisture content, the peak amplitude of the reflected signal is 0.1 v, whereas the peak amplitude of the reflected signal is 0.03 v in the lower moisture content soil.

The air cavity effect is noticed when comparing Figures 58 and 59. Both of these tests were conducted under approximately the same soil conditions. In Figure 58, the peak signal amplitude is 0.1 v and in Figure 59, the peak signal amplitude is 0.07 v. In Figure 58, the steel mine had top and bottom plates of 1/4-inch thick steel and an air cavity of approximately 1-3/8 inches. In Figure 59, the steel mine had top and bottom plates of 1/16-inch thick steel and an air cavity of approximately 3 inches. Compare the reflected signals of Figures 39 and 51; the soil moisture content, driving voltage and object depth are about the same in each case. In Figure 39, however, the object was two 1/4-inch steel plates which were bolted together with no air gap between the plates. The mine used in Figure 51 was the one with 1/4-inch steel plates with a 1-3/8-inch air cavity. Notice that the signal received in Figure 39 is considerably larger than the signal received in Figure 51. It appears that the strength of the reflected signal is a function of the mine material thickness and of the air cavity thickness present - the latter exhibiting a lesser effect.

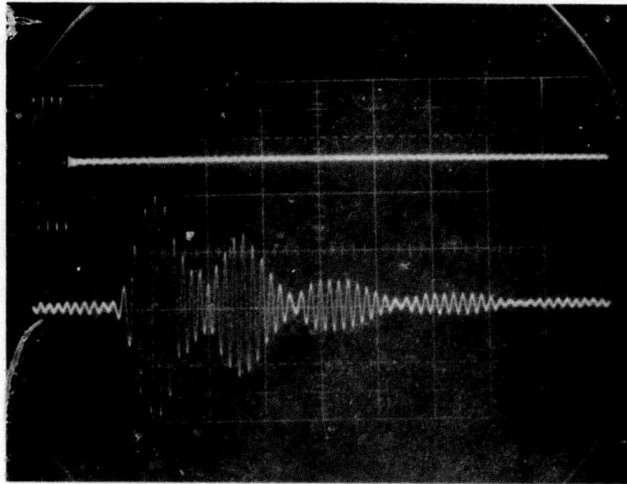


Figure 58: Reflected signal from steel mine with 1/4-inch plates at a depth of 9 inches. Top trace is input to transmitter, 500 v/division. Bottom trace is receiver output, 0.05 v/division. Horizontal scale: 2 msec/division.

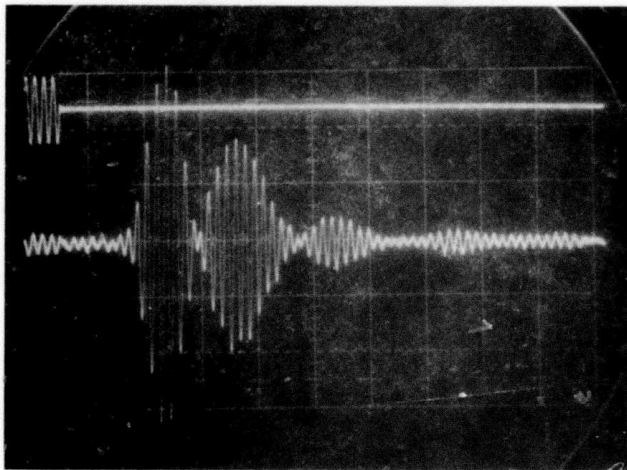


Figure 59: Reflected signal from steel mine with 1/16-inch plates at a depth of 9 inches. Top trace is input to transmitter, 500 v/division. Bottom trace is receiver output, 0.02 v/division. Horizontal scale: 2 msec/division.

The peak electrical power utilized to obtain the reflection signals was on the order of 30 watts. Although the input voltage was 424 volts (rms) the input impedance of the transducer resulted in only a small current drain. Since the transducer also has a reactance component, the power factor was considered in the calculation of input power. For the 3 KHz transducer, the manufacturer specified that a minimum of 60% of the electrical power would be converted into acoustic power. This would imply an acoustic radiated power of 18 watts. This efficiency rating was made for a transducer in a "free-field." Since the transducer was placed close to a large mass area (ground), mass loading effects may have reduced this efficiency. The mass loading effect on the resonant frequency is evident from the previous frequency amplitude spectrums. Notice that the spectrum for the 3 KHz (Figure 18) transducer has as its center frequency 2.55 KHz and not the 3 KHz frequency that was put in.

A primary factor influencing the amount of power that can be applied to the sound projecting transducer is cavitation. Cavitation is basically a property of the fluid medium into which the sound is radiated. Cavitation bubbles begin to form on the face and just in front of the transducer. These bubbles result from the rupture of water caused by negative pressures of the generated sound field. These negative pressures cause the liquid to tear apart when they exceed a cavitation threshold¹⁰. When the radiated power exceeds the cavitation threshold, several conditions result which significantly reduce the transducer's performance.

The transducer is rated at a maximum input power of 100 watts with a continuous wave (CW) signal. For this size transducer, cavitation in water would occur at an acoustic power of 27.4 watts at an ambient pressure of one atmosphere. This figure was calculated assuming cavitation occurs at 0.3 watts/cm^2 with a continuous wave signal in water⁹. The power level at which cavitation occurs is a function of (1) the radiating area of the transducer, (2) the local ambient pressure, (3) the viscosity of the liquid in which the transducer is immersed, and (4) the duration and frequency of the signal. None of these factors have been analytically correlated in the literature. Experimental studies have been made which indicate that

the cavitation threshold increases with increasing frequency and decreasing pulse width¹⁰. For the low frequency of 3 KHz, the CW cavitation threshold (in fresh water) is much lower than 0.3 watts/cm²; however, for a four cycle pulse width, the threshold is again raised to 0.3 watts/cm². The 3 KHz transducer was therefore driven at 65% of the power limit resulting in cavitation.

3.2 Acoustic Impedance

The acoustic impedance at a given surface is defined as the complex ratio of effective sound pressure averaged over the surface to effective volume velocity through it. The characteristic impedance is the ratio of the effective sound pressure at a point to the effective particle velocity at that point in a free, plane, progressive sound wave. It is equal to the product of the density of the medium times the speed of sound in the medium (ρc)⁵.

Since the density variation in a porous medium is not in phase with the pressure variation, the acoustic impedance is complex. In a compact solid medium, however, the two will be in phase. In this analysis, we will assume a very compact soil so that the characteristic impedance may be used to determine reflection and transmission coefficients.

The following characteristic impedances will be used in subsequent calculations (see Table IX).

Consider the transmission of a plane acoustic wave through three different media. Let the characteristic impedances of the media be given by $\rho_1 c_1$, $\rho_2 c_2$ and $\rho_3 c_3$, respectively (Figure 60).

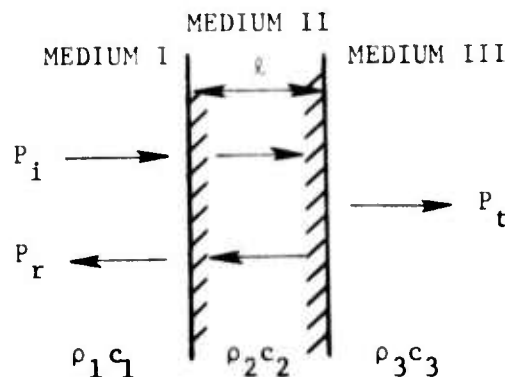


Figure 60: Transmission through a separating material.

TABLE IX. Characteristic Impedance

Material	ρ kg/m ³	c m/sec	Characteristic z = ρc MKS Rayls
Pine	450	3500	1.57×10^6
Water (20°C)	998	1481	1.48×10^6
Air	1.21	343	415
Concrete	2600	3100	8×10^6
Steel	7700	6100	47×10^6
Rubber (hard)	1100	2400	2.64×10^6
Lucite	1200	2650	3.2×10^6
Soil*	1765	152-213	$0.27-0.38 \times 10^6$

* Dependent on soil conditions

(Here $\rho = 110 \text{ lb/ft}^3$; $c = 500-700 \text{ ft/sec}$)

The sound power transmission coefficient, α_t , from medium I through medium II and into medium III is

$$\alpha_t = \frac{4\rho_3 c_3 \rho_1 c_1}{(\rho_3 c_3 + \rho_1 c_1)^2 \cos^2 k_2 \ell + (\rho_2 c_2 + \rho_3 c_3 \rho_1 c_1 / \rho_2 c_2)^2 \sin^2 k_2 \ell} \quad (3.2.1)$$

where $k_2 = \omega/c_2$ and ℓ = width of medium II. This equation can be used to estimate the amount of acoustic power radiated from the fluid coupling medium, through the pliable coupling membrane and into the soil. If the pliable membrane is a rubber, Table X lists the sound power transmission coefficient for various thicknesses, assuming a soil characteristic impedance of 0.325×10^6 MKS rayls. The sound power reflection coefficient is given by

$$\alpha_r = 1 - \alpha_t \quad (3.2.2)$$

This coefficient represents the ratio of reflected power to incident power in medium I.

TABLE X. Transmission from Water through Rubber into Soil at a Frequency of 3 KHz.

Material	$\rho_2 c_2$ MKS rayls	c_2 m/sec	ℓ inches	α_t	α_r
Rubber (hard)	2.64×10^6	2400	0.5	0.58	0.42
			0.25	0.59	0.41
			0.125	0.59	0.41
Rubber (soft)	1.0×10^6	1050	0.5	0.60	0.40
			0.25	0.59	0.41
			0.125	0.59	0.41
Rubber (ρc)	1.55×10^6	1550	0.5	0.38	0.62
			0.25	0.59	0.41
			0.125	0.59	0.41

Note that for rubber thicknesses ≤ 0.25 inch no matter which type of rubber is chosen, the sound power transmitted into the soil is 59% of the incident acoustic power. This result is the same as would be obtained at a soil-water boundary. The thin rubber membrane is essentially acoustically transparent. The transmission loss is solely due to the impedance mismatch between the water and the soil.

If we assume that a buried mine is a solid block of some material, then equations 3.2.1 and 3.2.2 can be used to estimate the amount of power reflected at the mine relative to the incident signal. The sound power reflection coefficients are listed in Table XI for mines made of pine, steel, lucite and other mine materials. Since soil is on both sides of the mine,

$$\rho_1 c_1 = \rho_3 c_3$$

Then the sound power transmission coefficient is

$$\alpha_t = \frac{4}{4 \cos^2 k_2 \ell + \left(\frac{\rho_2 c_2}{\rho_1 c_1} + \frac{\rho_1 c_1}{\rho_2 c_2} \right)^2 \sin^2 k_2 \ell} \quad (3.2.3)$$

TABLE XI. Sound Power Reflection Coefficient for Mines Buried in Soil.

Material	$\rho_2 c_2$ MKS rayls	c_2 m/sec	l inches	α_t^*	α_r^*
Pine	1.57×10^6	3500	6	0.26	0.74
			2	0.72	0.28
Steel	47×10^6	6100	3	0.0035	0.996
			0.25	0.34	0.66
			0.0625	0.999	0.001
Lucite	3.2×10^6	2650	5	0.064	0.94
Cast Iron	33.5×10^6	4350	3	0.0036	0.996
Aluminum	17×10^6	6300	3	0.0277	0.972
Lead	23.2×10^6	2050	3	0.0019	0.998
Concrete	8.0×10^6	3100	4	0.0194	0.98
Air	415	331.6	0.5	2.2×10^{-5}	1
			1	7.8×10^{-6}	1
			3	6.82×10^{-5}	1

* Frequency is 3 KHz.

It is evident from Table XI that, for the materials listed, most of the incident power on the mine would be reflected. In actuality mines are not made of solid blocks of material. Mines do, however, often contain small air cavities between the top layer of explosive and the top plate of the mine. From Table XI we see that even a small segment of air in soil acts as a perfect reflector of sound. Now let us calculate the amount of sound power reflected from a thin piece of material (in soil) backed by air. Figure 61 illustrates the situation to be considered. Utilizing equations 3.2.1 and 3.2.2, we can then calculate the sound power reflection coefficient. These results are listed in Table XII. By comparing the results of Tables XI and XII we note that the presence of an air cavity within the mine significantly increases the acoustic reflectivity of the mine.

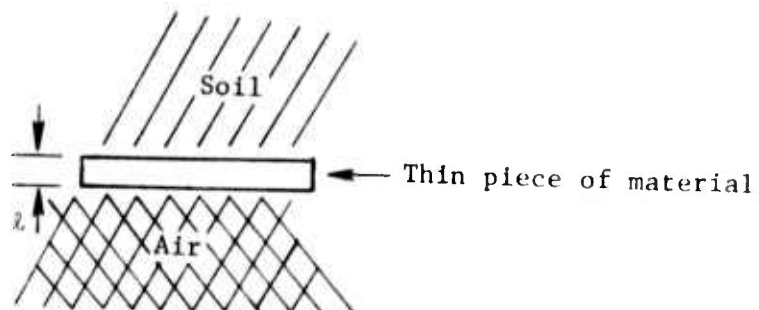


Figure 61: Thin piece of material with soil on one side and air on the opposite side.

TABLE XII. Sound Power Reflection Coefficient for Thin Mine Material with Soil on One Side and Air on the Opposite Side.

Material	l inches	α_t^*	α_r^*
Pine	2	0.00194	0.998
	1	0.00362	0.996
Steel	0.25	0.00059	0.999
	0.0625	0.00324	0.997

* At a frequency of 3 KHz.

4.0 REFERENCES

1. Hardin, B. O., and F. E. Richart, "Elastic Wave Velocities in Granular Soils," Journal of the Soil Mechanics and Foundations Division, ASCE, SMI, pp. 33-65, February 1963.
2. Paterson, N. R., "Seismic Wave Propagation in Porous Granular Media," Geophysics, Vol. 21, No. 3, pp. 681-714, July 1956.
3. Biot, M. A., "Generalized Theory of Acoustic Propagation in Porous Dissipative Media," J. Acoust. Soc. Am., Vol. 35, No. 9, pp. 1254-1264, September 1962.
4. Nyborg, W. L., I. Rudnick and H. K. Schilling, "Experiments on Acoustic Absorption in Sand and Soil," J. Acoust. Soc. Am., Vol. 22, No. 4, pp. 422-425, July 1950.
5. Beranck, L. L., Acoustics, McGraw-Hill, N.Y., 1954.
6. Lambe, T. W., Soil Mechanics, John Wiley & Sons, Inc., N.Y., 1969.
7. Kinsler, L. E., and A. R. Frey, Fundamentals of Acoustics, John Wiley & Sons, Inc., N.Y., 2nd ed., 1962.
8. Zwicker, C., and C. W. Kosten, Sound Absorbing Materials, Elsevier Publishing Company, Inc., N.Y., 1949.
9. Albers, V. M., Underwater Acoustics Handbook II, Pennsylvania State University Press, Pennsylvania, 1965.
10. Urick, R. J., Principles of Underwater Sound for Engineers, McGraw-Hill Book Co., Inc., N.Y., 1967.

DOCUMENT CONTROL DATA - R & D

(Security classification of title, body of abstract and indexing annotation must be entered when the overall report is classified)

1. ORIGINATING ACTIVITY (Corporate author) TRW Systems Group One Space Park Redondo Beach, California 90278		2a. REPORT SECURITY CLASSIFICATION Unclassified	
		2b. GROUP	
3. REPORT TITLE LAND MINE DETECTION SYSTEM			
4. DESCRIPTIVE NOTES (Type of report and inclusive dates) Final Report, 1 April 1972 - 15 February 1973			
5. AUTHOR(S) (First name, middle initial, last name) Allen M. Morita			
6. REPORT DATE 23 February 1973		7a. TOTAL NO OF PAGES 80	7b. NO OF REFS 10
8a. CONTRACT OR GRANT NO. DAAK02-72-C-0340		9a. ORIGINATOR'S REPORT NUMBER(S) Advanced Technology Staff/ Space Vehicles Division Report No. AT-73-2	
b. PROJECT NO		9b. OTHER REPORT NO(S) (Any other numbers that may be assigned this report)	
c.			
d.			
10. DISTRIBUTION STATEMENT			
11. SUPPLEMENTARY NOTES		12. SPONSORING MILITARY ACTIVITY U.S. Army Mobility Equipment Research and Development Center, Ft. Belvoir, Va. 22060	
13. ABSTRACT The objective of this contract was to determine the feasibility of using acoustic waves for the detection of metallic and nonmetallic land mines. It was found that a 3 KHz pulse burst could detect all of the simulated mines at burial depths exceeding 12 inches. The mine reflected signals exhibited a signature significantly different from those obtained with no mine present and with small soil inhomogeneities present. Rock reflected signals generally exhibited irregular axes of reflection. Mine reflected acoustic signals can be detected and imaged from both nonmetallic and metallic mines at the burial depths most likely occurring in a field situation.			

14 KEY WORDS	LINK A		LINK B		LINK C	
	ROLE	WT	ROLE	WT	ROLE	WT
Mine Detection Acoustics						